

Dermo-DOCTOR: A framework for concurrent skin lesion detection and recognition using a deep convolutional neural network with end-to-end dual encoders

Md. Kamrul Hasan^{a,1,*}, Shidhartho Roy^a, Chayan Mondal^a, Md. Ashraful Alam^a, Md. Toufick E Elahi^a, Aishwariya Dutta^b, S. M. Taslim Uddin Raju^c, Md. Tasnim Jawad^a, Mohiuddin Ahmad^a

^a*Department of Electrical and Electronic Engineering, Khulna University of Engineering & Technology, Khulna-9203, Bangladesh*

^b*Department of Biomedical Engineering, Khulna University of Engineering & Technology, Khulna-9203, Bangladesh*

^c*Department of Computer Science and Engineering, Khulna University of Engineering & Technology, Khulna-9203, Bangladesh*

Abstract

Background and Objective

Automated skin lesion analysis for simultaneous detection and recognition is still challenging for inter-class homogeneity and intra-class heterogeneity, leading to low generic capability of a Single Convolutional Neural Network (CNN) with limited datasets.

Methods

This article proposes an end-to-end deep CNN-based framework for simultaneous detection and recognition of the skin lesions, named Dermo-DOCTOR, consisting of two encoders. The feature maps from two encoders are fused channel-wise, called Fused Feature Map (FFM). The FFM is utilized for decoding in the detection sub-network, concatenating each stage of two encoders' outputs with corresponding decoder layers to retrieve the lost spatial information due to pooling in the encoders. For the recognition sub-network, the outputs of three fully connected layers, utilizing feature maps of two encoders and FFM, are aggregated to obtain a final lesion class. We train and evaluate the proposed Dermo-Doctor utilizing two publicly available benchmark datasets, such as ISIC-2016 and ISIC-2017.

Results

The achieved segmentation results exhibit mean intersection over unions of 85.0% and 80.0% respectively for ISIC-2016 and ISIC-2017 test datasets. The proposed Dermo-DOCTOR also demonstrates praiseworthy success in lesion recognition, providing the areas under the receiver operating characteristic curves of 0.98 and 0.91 respectively for those two datasets. The experimental results show that the proposed Dermo-DOCTOR outperforms the alternative methods mentioned in the literature, designed for skin lesion detection and recognition.

Conclusion

As the Dermo-DOCTOR provides better-results on two different test datasets, even with limited training data, it can be an auspicious computer-aided assistive tool for dermatologists.

Keywords: Malignant melanoma, Skin lesion detection and recognition, Convolutional neural networks, Dual encoder networks, ISIC skin lesion datasets.

1. Introduction

1.1. Problem Presentation

Cancer is an abnormal and uncontrolled growth of dividing cells, damaging different body cells and contributing to the world's second-leading cause of death [76]. Although melanomas constitute less than 5.0% of all skin cancers, they make up about 75.0% of deaths related to skin cancer in the United States (US) alone [18]. Age-standardized melanoma rates of the top 20 countries [9] is presented in Fig. 1. According to the world health organization, 466914 new cases of skin cancer will be diagnosed in 2040 (54.27% men and 45.73% women), and 105904 (58.14% men and 41.86% women) will die. The five-year survival rate of melanoma,

*I am corresponding author

Email addresses: m.k.hasan@eee.kuet.ac.bd (Md. Kamrul Hasan), swapno15roy@gmail.com (Shidhartho Roy), chayan.eee.92@gmail.com (Chayan Mondal), ashrafalalam16e@gmail.com (Md. Ashrafal Alam), toufick1469@gmail.com (Md. Toufick E Elahi), aishwariyadutta16@gmail.com (Aishwariya Dutta), taslimuddinraju7864@gmail.com (S. M. Taslim Uddin Raju), jawad1703006@stud.kuet.ac.bd (Md. Tasnim Jawad), ahmad@eee.kuet.ac.bd (Mohiuddin Ahmad)

¹Department of EEE, KUET, Khulna-9203, Bangladesh.

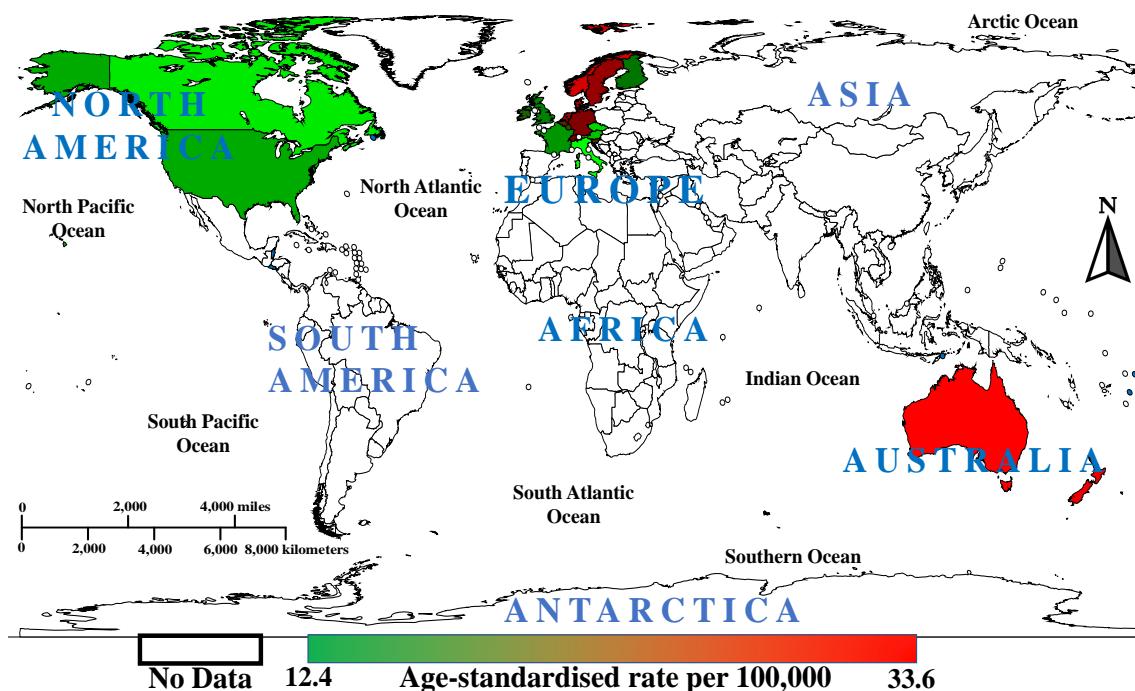


Figure 1: A world heat map of the age-standardized rates per 1.0 million population of the top 20 countries with the highest skin melanoma rates in 2018 [9], displaying highly skin cancer affected regions.

the deadliest variety of early detection, is as high as 99.0%, but delayed diagnosis leads significantly to a colorectal survival rate decrease of 23.0% [84]. However, reliable early identification is highly imperative as the five-year survival rate will be increased by 90.0% approximately [23]. Dermatologists generally examine images via naked-eye through visual examination, requiring a high level of expertise and focus. The manual inspection by dermatologists is often very tiresome, time-consuming, subjective, and fault-prone. The precision of skin lesions' diagnosis by the dermatologists suffers from inter-class homogeneity and intra-class heterogeneity. Moreover, the ratio of dermatologists per 1.0 million population in the US, South Australia, and Europe are respectively 34.0, 26.0, and 59.34, which are very low compared to the required numbers [15, 16, 26]. However, an automated Computer-aided Screening (CAS) system has become popular among dermatologists to alleviate the above limitations, reduce the working burden of dermatologists, and accelerate diagnosis rates [50]. Such CAS systems essentially consist of several integral parts, where the segmentation for Region of Interest (ROI) extraction and the classification for lesion recognition. However,

image-based automated CAS systems are highly challenging for the following hurdles:

- Wide range of intra-class variance in colors, textures, edges, and shapes and homogeneity in inter-classes.
- Sometimes, low contrasts and unclear boundaries (edges) in the malignant and other class images.
- Lesion ROI frequently shares similar visual characteristics and subtle distinctions due to lighting, perspective, and spatial information within an image.
- The appearance of different artifacts, such as natural (hairs, veins) or synthetic (air bubbles, ruler lines, color balance charts, marker signs, paint, ink color, artificial objects, *etc.*), LED lighting, darker border (microscopic effects), and non-uniform vignetting, as depicted in Fig. 2.
- Lesion ROI only covers a small proportion of local, subtle grain, and global context information.
- Unavailability of a large number of manually annotated images, which is the core requirement of the supervised learning systems.

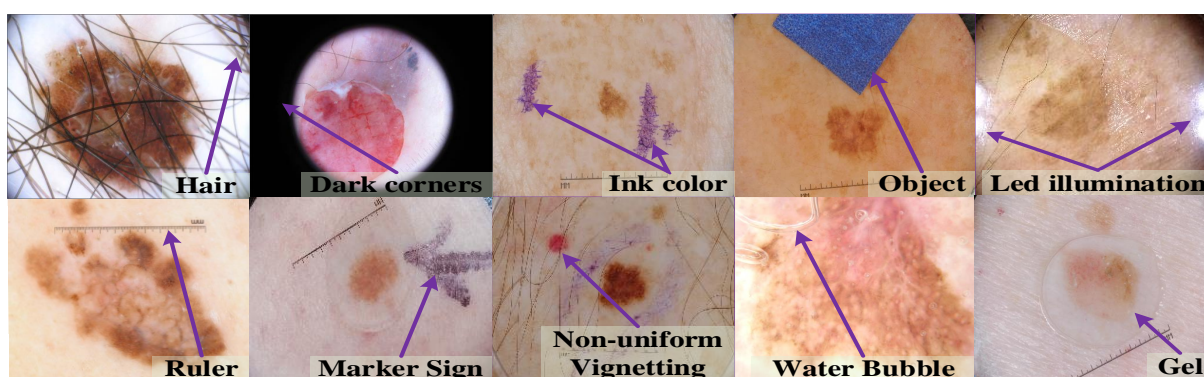


Figure 2: An example of the challenging dermoscopic images in ISIC dataset [13, 29] with different artifacts [35].

1.2. Recent Methods

The state-of-the-art methods for skin lesion segmentation and recognition are reviewed and described in the following two subsections.

1.2.1. Methods for Lesion Segmentation

A multi-stage Fully Convolutional Network (mFCN) with parallel integration was introduced by Bi et al. [8]. During the training process, mFCN learned from both the training data and the coarse results obtained from the previous (m-1)FCN stage. The summation of the earlier results with the current result had two benefits: boost the training data and optimize lesion boundary learning. Navarro et al. [62] proposed a superpixels adaptation-based segmentation approach to get tight-to-boundaries of the skin lesions. The authors applied the Scale-Invariant Feature Transform (SIFT) [54] and Gaussian distribution to detect the feature points and place these points to the initial centers. Finally, they applied the simple linear iterative clustering technique to these points for generating the final lesion masks. An encoder-decoder network was built by Sarker et al. [71], called SLSDeep. The encoder in SLSDeep was dilated residual network-based design, while the decoder had a pyramid pooling network. Additionally, they proposed a combined negative log-likelihood and end-point error-based cross-entropy loss function. Jahanifar et al. [45] developed an improved saliency detection supervised method for the lesion segmentation, which was designed based on the discriminative regional feature integration. They used a thresholding algorithm for generating a new pseudo background region. Goyal et al. [27] designed an automatic ensemble of DL methods, such as DeeplabV3+ [19] and Mask R-Convolutional Neural Network (R-CNN) [38], for generating the precise lesion boundaries. They combined the result of two models in three ways: a combination of both masks, picking the larger segmented area from the output of both methods, and picking a smaller area from those outputs. Finally, the authors discovered that the first method outperforms the other ensembling methods. Al-Masni et al. [2] proposed a Full Resolution Convolutional Network (FrCN) for the skin lesion segmentation, which learns full resolution features from each pixel of an input image. A segmentation method is realized by Hawas et al. [36] for the neutrosophic graph

cut algorithm. The initial clusters were obtained using Histogram-based Clustering Estimation (HBCE) with the corresponding centroids. The genetic algorithm was applied to optimize the HBCE for getting the optimal threshold. Then, the Neutrosophic C-means (NCM) mapped the lesions into a Neutrosophic Set (NS) domain. Finally, for the lesion segmentation, the graph cut algorithm was a cost function. Amin et al. [5] segmented the lesion in two steps. In the first step, the authors performed preprocessing to resize the images to $240 \times 240 \times 3$ and convert the RGB into *Lab* to select the luminance channel. Finally, in the second step, biorthogonal $2D$ wavelet transform and OTSU algorithm were applied for the lesion segmentation. Xie et al. [86] produced a deep CNN, called mutual bootstrapping deep CNN (MB-DCNN). MB-DCNN has three networks, such as a coarse segmentation network (coarse-SN), a mask-guided classification network (mask-CN), and an enhanced segmentation network (enhanced-SN). Coarse-SN was used to roughly segment the lesion and feed the label region to mask-CN to boost the classification task. Al Nazi and Abir [4] compared the performance of two variations of the UNet [70] model for the lesion segmentation, such as UNet without spatial dropout and UNet with spatial dropout. In the end, the authors showed that augmentation and dropout, as regularization methods, with UNet, had less prone to overfitting and provided better-segmented lesion masks. Pour and Seker [67] offered a segmentation model based on CNN with CIELAB color space and transformed domain feature extraction. The authors initially implemented a scratch model inspired by UNet and FCN, then gradually improved the model by injecting features from the transformed domain and adding the input image color model CIElab. They succeeded in coping with the constraints that included small data set, removal of artifacts, excessive data increase, and contrast stretching. They also confirmed that the CNN model’s performance with a domain transfer feature is better than the CNNs with a deep layer network.

1.2.2. Methods for Lesion Recognition

Many image analysis-based methods have already been proposed and developed by the researchers for dermoscopic image recognition, where the algorithms generally depend on the detection and extraction of low-level handcrafted features, such as colors, shapes, tex-

tures, and *etc.* Cheng et al. [11] extracted different features from the first-order histogram probability such as area, roundness (thinness), mean, standard deviation, skew, energy, and entropy. Finally, the authors applied different classifiers, namely quadratic discriminant analysis and Multilayer Perceptron (MLP), on the selected features by the Principal Components Analysis (PCA) [55]. Different visual cues, such as ABCD (Asymmetry, Border, Color, and Differential structures) rule of dermoscopy [61], texture (neighboring gray-level dependence matrix, angular second-moment, and kinetics of skin lesions) were extracted by Maglogiannis and Doukas [56]. The authors also selected the features using the sequential backward floating selection, PCA, and generalized sequential feature selection algorithms. Finally, they employed MLP and Support Vector Machine (SVM) [21] for the lesion classification. Oliveira et al. [64] computed different local features employing the bag-of-features [25] approach and texture features, where the authors selected the subset of features using a heuristic search approach. In the end, they applied SVM, Bayesian network, Decision Tree (DT) [1], and Artificial Neural Network (ANN) as classifiers. Hameed et al. [31] developed an intellectual Multi-Class Multi-Level (MCML) classification algorithm employing two approaches, such as traditional machine learning and deep learning. In the former method, they applied preprocessing, segmentation, extraction of features, and classification. As a preprocessing, they removed the hair, black frames, and circle. Finally, the authors classified the texture and color features employing the ANN. Mporas et al. [60] applied a median filter followed by bottom-hat filtering to detect natural hair or similar to hair artifacts. They segmented the ROIs using the active contour model on the grayscale image. Finally, they extracted different color-based features for classification using the MLP and other Machine Learning (ML) algorithms.

However, as described earlier, the lesion classification algorithms are very complex as they essentially rely on the handcrafted features extraction method, requiring prior knowledge [20] and lots of parameter tuning. Extensive feature engineering is the key to achieving better-performance from them, which is often impossible due to the presence of different artifacts in the dermoscopic images (see in Fig. 2). The development of various CNN-based classifiers has achieved a remarkable result on the ImageNet dataset [14]. Nowadays, in many

computer vision problems, the contribution of both CNNs and DL techniques are undeniable [28]. CNN is an excellent feature extractor, which necessarily alleviates the manual feature engineering as in the algorithms mentioned above, therefore applying it to recognize medical images [87]. Mahbod et al. [57] presented an ensemble-based model for CNNs that combines inter-and intra-architecture network fusion. The authors applied the fine-tuning of pre-trained VGGNet, AlexNet [48], and two types of ResNet. Finally, the average prediction probability classification vectors from different sets were fused to provide the final prediction. Brinker et al. [10] exercised ResNet-50 with transfer learning [82]. For the optimization of the model, they adopted three techniques. Firstly, they exclusively trained the adapted last layer, then fine-tuned all layers' parameters, and finally, a sudden increment of the learning rate at specific time steps during fine-tuning. Zhang et al. [91] presented an Attention Residual Learning (ARL) CNN model for the skin lesion recognition, which was composed of multiple ARL blocks, a global average pooling, and a classification layer. Each ARL block employed residual learning and novel attention learning mechanisms to improve its capability for discriminative representation. The authors proposed the attention learning mechanism, which aimed to utilize the intrinsic self-attention ability of DCNNs, i.e., using the feature maps learned from a high layer to generate a low-layer attention map instead of applying extra learnable layers. An integrated framework for skin lesion boundary detection as well as for skin lesions classification was described by Al-Masni et al. [3]. Firstly, a deep learning method, named FrCN, was used for the lesion boundary extraction. Then, geometric augmentation and transfer learning were integrated with four CNN networks, such as Inception-V3 [79], ResNet-50, Inception-ResNet-V2, and DenseNet-201 [42] for the lesion classification. They also showed that segmented lesions improve lesion classification results. Yilmaz and Trocan [88] implemented three deep CNN models named AlexNet, GoogLeNet, and ResNet-50. They compared classification performance as well as time complexity of the implemented models. For data augmentation, a style-based Generative Adversarial Network (GAN) architecture was proposed by Qin et al. [68]. In the end, the authors applied ResNet-50, with transfer learning, for the lesion classification. Khan et al. [47] proposed a model for the lesion classification, which included the localization of lesion

ROI via faster region-based CNN, feature extraction, and feature selection by iteration-controlled Newton-Raphson method. The ABC-based method was first used for contrast stretching and then used for lesion segmentation. DenseNet-201, via transfer learning, was used to extract deep-level features, and those features were classified using an MLP. Gessert et al. [24] ensembled different DL methods, such as EfficientNets [80], SENet [41], and ResNeXt, by a selection strategy. They used multi-resolution input by multi-crop evaluation and two different cropping strategies. The encoding of metadata as a feature vector was concatenated with the dense (fully connected) neural network. Valle et al. [83] optimized the hyperparameter of two deep CNN models, ResNet-101-V2, and Inception-V4 employing transfer learning with data augmentation. They select the best performing classifier using the ANOVA test [73]. Finally, the authors concluded that the transfer learning and ensembling model is a better choice for lesion classification.

1.3. Our Contribution

The above-discussions on the automatic skin lesion diagnosis methods confirm that the deep CNN approaches are commonly applied nowadays than the different systems relying on handcrafted features. The former approaches provide good reproducibility of results and boost diagnostic procedures' speed while being end-to-end methods. However, the CNN-based skin lesion analysis methods suffer from data scarcity to evade overfitting. The ensembling of different CNN architectures can mitigate those CNN's limitations, as proven by Harangi [32]. In many articles [24, 27, 30, 32, 51, 58, 66, 75], the authors first trained different CNN models independently and then aggregated their outputs for developing ensembling models. Such an ensembling is tedious and time-consuming, leading to massive time and resources for training and testing. However, to eradicate those limitations, an end-to-end ensemble approach for skin lesion analysis without compromising state-of-the-art outcomes is highly essential. With the aforementioned thing in mind, this article aims to provide the following contributions:

- Develop an end-to-end ensembling model with dual encoders in our Dermo-DOCTOR framework, concatenating two different feature maps from those two encoders to

broaden the lesion’s depth information. Such a proposed network with two different encoders with the same input is likely to learn more discriminating features with limited training samples.

- Incorporate segmented lesion ROIs for the recognition as ROIs enable the classifier to learn the abstract region and detailed structural description while avoiding surrounding healthy regions.
- Apply geometry- and intensity-based image augmentations and transfer learning to alleviate overfitting; the class rebalancing techniques to protect the classifier from being biased towards any particular class with more samples.
- Develop and compare two other networks for detection (UNet and FCN8s) and recognition (ResNet-50 and Xception [12]) under the same experimental settings.
- Demonstrate state-of-the-art lesion detection and recognition results, to our best knowledge, on two IEEE International Symposium on Biomedical Imaging (ISBI) datasets, such as ISIC-2016 and ISIC-2017, having a different number of classes.
- Implement a possible application of our Dermo-DOCTOR, deploying its trained weights, which runs in a web browser (see in YouTube²).

The rest of the paper is structured accordingly. We explain the design of the Dermo-DOCTOR framework and datasets in section 2. The results and discussions of the extensive experiments, with the proper interpretation, are reported in section 3. Finally, we conclude the article in section 4.

2. Materials and Methods

This section manifests the materials and methods, describing the proposed Dermo-DOCTOR pipeline in Section 2.1. We explain the utilized datasets, integral preprocessing,

²Dermo-DOCTOR App: <https://bit.ly/Dermo-DOCTOR>

and the proposed network in Subsections 2.1.1, 2.1.2, and 2.1.3, respectively. Sections 2.2 and 2.3 respectively describe our web application and network’s training protocol.

2.1. Proposed Framework

The overall Dermo-DOCTOR framework is illustrated in Fig. 3. We utilize two different

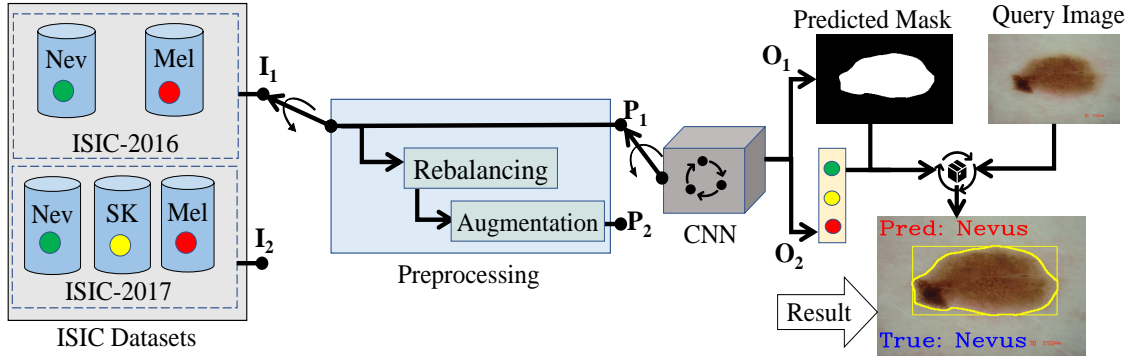


Figure 3: The proposed pipeline for concurrent detection and recognition systems, where the preprocessing has incorporated with the proposed network to build a precise diagnostic system. An input I_1 or I_2 generates two outputs O_1 and O_2 , where O_1 and O_2 respectively denote the segmentation and recognition results.

input types (either I_1 or I_2), where I_1 or I_2 is a binary or a multi-class categorization task. An input, either I_1 or I_2 , generates two different outputs, such as segmentation (O_1) and recognition (O_2). The outputs O_1 and O_2 are then processed to provide lesion detection and recognition results. We process the predicted lesion masks to generate the bounding box around the lesion, naming lesion detection. However, different crucial integral parts of the Dermo-DOCTOR are explained in the following subsections.

2.1.1. Datasets

Two different datasets, such as ISIC-2016 [29] and ISIC-2017 [13], are used to validate our proposed pipeline, whose class-wise distributions are presented in Fig. 4. The ISIC-2016 contains a binary class, aiming to classify as either Nevus (Nev) or Melanoma (Mel), explicating that class samples are imbalanced (4.2 : 1 for $Nev : Mel$). On the other hand, the ISIC-2017 is a multi-class categorization task, intending to classify as either Nevus (Nev), or Seborrheic Keratosis (SK), or Melanoma (Mel). The distribution of ISIC-2017

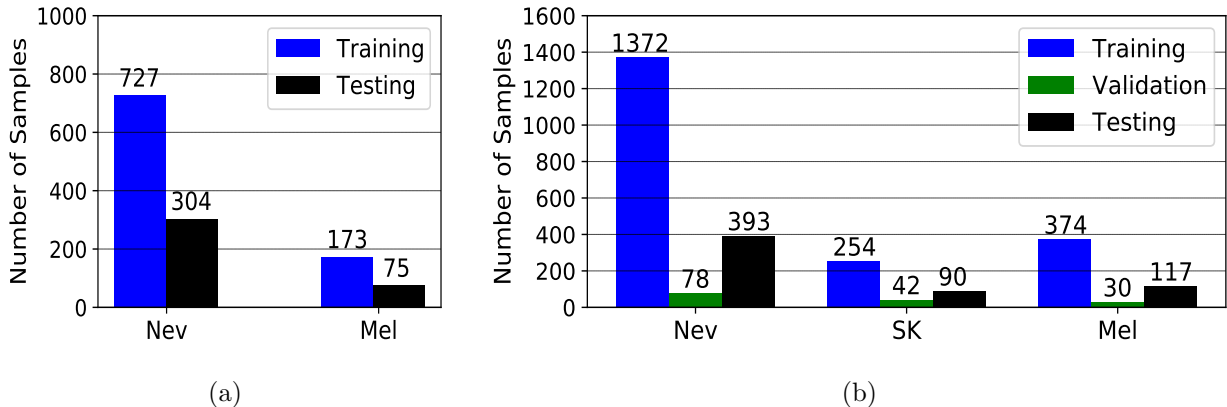


Figure 4: The distributions of the utilized ISIC datasets, where (a) is for ISIC-2016 and (b) is for ISIC-2017. The validation set for the ISIC-2016 is not available publicly (see in the left figure).

also tells that class samples are highly imbalanced, where $Nev : SK : Mel$ in the training set is $11.8 : 2.8 : 1$. The training samples' imbalanced distribution makes the classifier biased towards the particular class with more samples, mitigated in the proposed pipeline by adopting two techniques (see in subsection 2.1.2).

2.1.2. Preprocessing

We have applied class rebalancing and different image augmentations (both geometry- and intensity-based) as a preprocessing, which are concisely explained as follows:

Rebalancing. The class imbalance is a common phenomenon in the medical imaging domain as manually annotated images are very complex and arduous to achieve [32]. Such a class imbalance can be partially overcome using two commonly used approaches, such as the data-level method and algorithmic level method [37]. We have combined additional images to the underrepresented class from the ISIC archive [44] and weighted the loss function. For weighing the loss function, we apply $W_i = N_i/N$, where W_i , N , and N_i are the weight for i^{th} class, the total sample numbers, and the sample numbers in the i^{th} class, respectively.

Augmentation. One of the crucial challenges in the medical imaging domain is coping with the small datasets, such as in the ISIC datasets [32]. However, we have applied different augmentations based on geometric transformations, such as rotation, flipping, shifting,

zooming, and image processing functions, such as gamma, logarithmic, sigmoid corrections, and stretching, or shrinking the intensity levels.

However, the input I_1 or I_2 produces the lesion recognition output by applying two preprocessing types: the P_1 : only segmentation and the P_2 : rebalancing and augmentation with segmentation.

2.1.3. Proposed Network

Nowadays, CNN-based methods outperform the radiologists with high values of balanced accuracy as proven in [46, 69]. Nevertheless, they trained the models with an enormous number of annotated images. However, CNNs may be obliquely limited when employed with highly variable and distinctive image datasets with limited samples and having inter-class homogeneity and intra-class heterogeneity, as in dermoscopic ISIC datasets [13, 29]. Ensembling the network is likely to alleviate data scarcity limitation for the CNN training [17, 32, 49, 59, 72]. In this context, we propose a CNN-based end-to-end ensemble network for simultaneous lesion detection and recognition, consisting of two encoders, a decoder, and three Fully-connected Layers (FCLs), as shown in Fig. 5. The different parts of the proposed dual encoder network are explained in the following paragraphs.

Encoder-1. The first encoder (f^{en-1}) in the proposed network is presented in Fig. 6. It includes Identity (Iden) and Convolutional (Conv) blocks, applying the skip connections [40] in both blocks. There are two main advantages of such a skip connection. Firstly, the lack of regularization of the new layers does not affect their performance, and secondly, the new layers are not nil even when they are regulated. In encoder-1, an input convolution is adopted before Iden and Conv blocks, followed by a max-pooling. By stacking these blocks on top of each other, encoder-1 has been designed for getting a lesion feature map (see in Fig. 6). The output feature map of the encoder-1 is defined as $X_{en-1} = f^{en-1}(I_{in})$, where $X_{en-1} \in \mathcal{R}^{B \times H \times W \times D}$, and B , H , W , D , and I_{in} respectively denote the batch size, height, width, depth (channel), and input batch of images. The encoder-1 is divided into five sub-blocks (E_{1n} and $n = 1, 2, \dots, 5$), while the input image resolutions in each sub-block are down-sampled in half of the input resolutions. In the segmentation sub-network, each

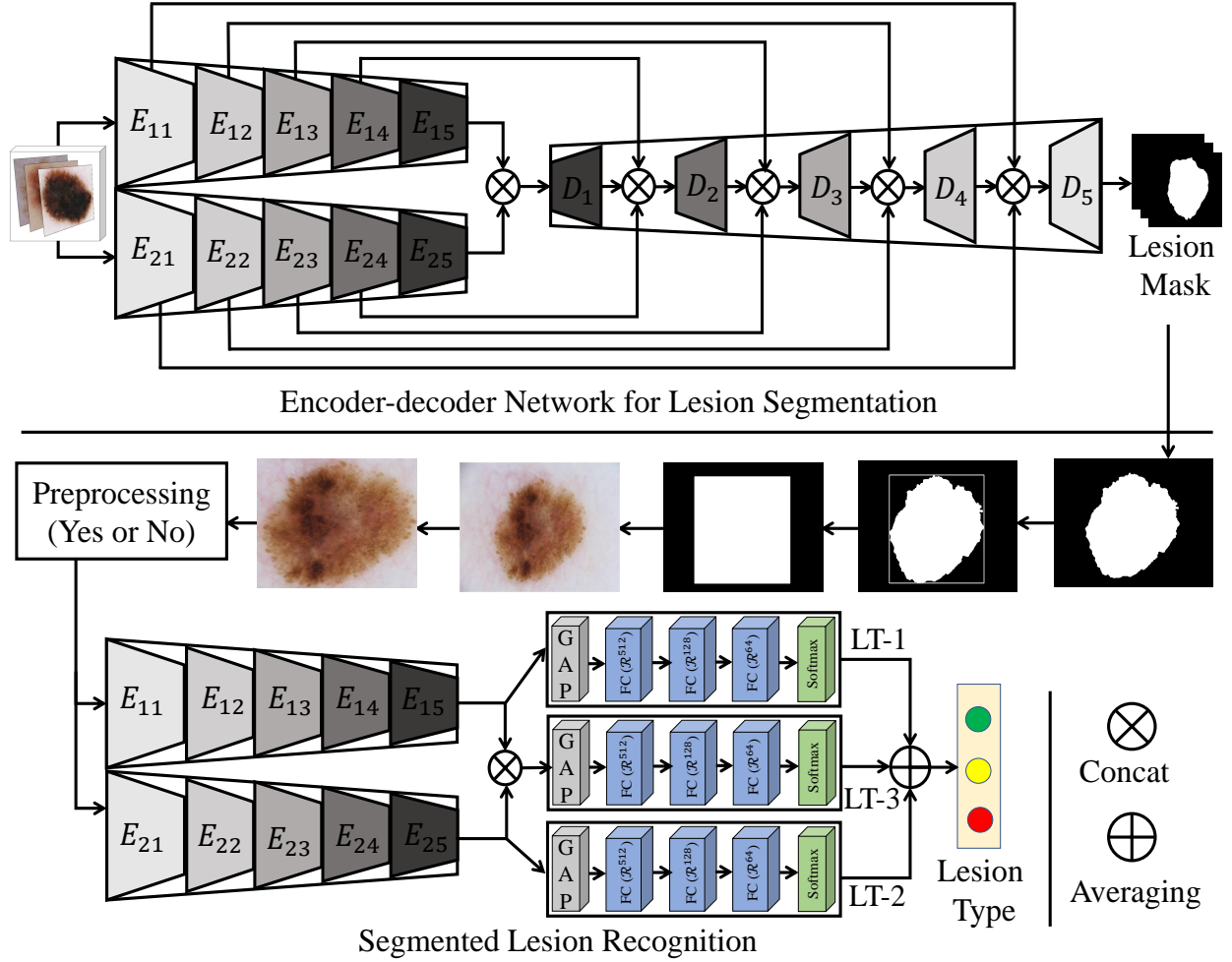


Figure 5: The proposed network for the Dermo-DOCTOR application, where the first encoder-decoder sub-network is applied for the lesion segmentation, while the second sub-network is employed for the lesion recognition. The segmented lesion masks are used for ROI extraction for further classification and detection utilizing the bounding boxes around the lesions.

sub-block’s outputs (E_{1n} and $n = 1, 2, \dots, 5$) will be used as an input for the skip connections to regain the lost spatial information due to pooling in the encoders.

Encoder-2. Within the encoder-2 (f^{en-2}), three block components are employed, such as entry flow, middle flow, and exit flow [12]. Fig. 7 depicts the constructional details of the encoder-2. The batch of input images firstly passes through the input flow, then the central flow, repeated eight times ($8\times$), and finally through the exit flow. All flows employ Depth-wise Separable Convolution (DwSC) [12] and residual connections. The former has been

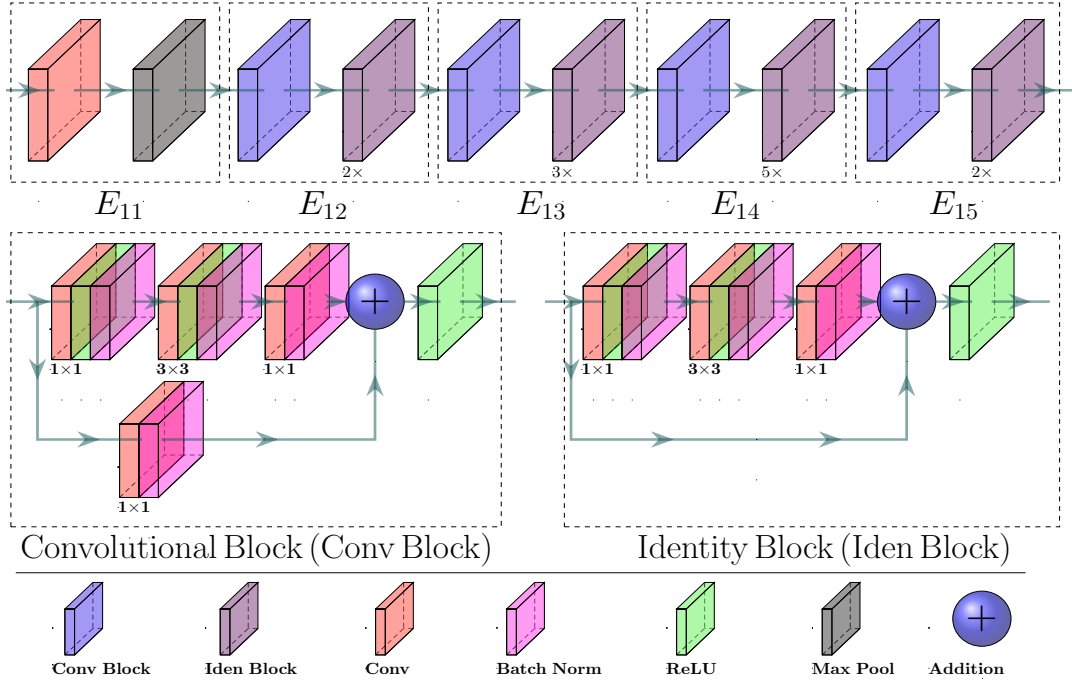


Figure 6: The encoder-1 of the proposed network, where the Conv and Iden blocks are stacked on top of each other. The notation ($n\times$) under the Iden block denotes the number of repetitions (n -times).

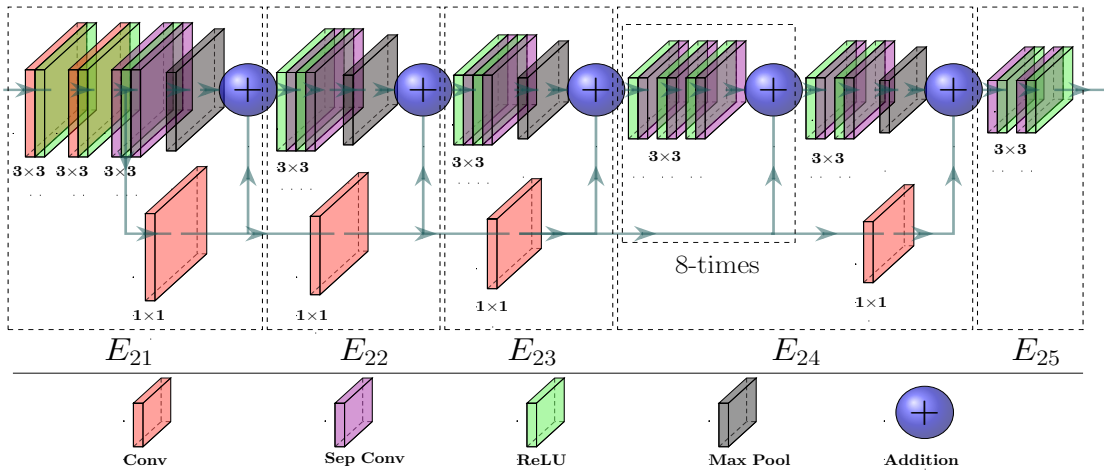


Figure 7: The encoder-2 of the proposed network, where depth-wise separable convolutions [12] were employed instead of traditional convolutions to make it lightweight for real-time applications.

used to create a lightweight network, while the latter has the advantages discussed earlier in encoder-1. The output feature map of the encoder-2 is defined as $X_{en-2} = f^{en-2}(I_{in})$, where $X_{en-2} \in \mathcal{R}^{B \times H \times W \times D}$, and B , H , W , D , and I_{in} respectively denotes batch size, height, width, depth (channel), and input batch of images. The encoder-2 is also divided into five sub-blocks (E_{2n} and $n = 1, 2, \dots, 5$), in which input resolutions are also down-sampled into half the resolutions of each sub-block. Every sub-blocks (E_{2n} and $n = 1, 2, \dots, 5$) are then used as the skip connections, when it is decoded in the detection sub-network.

Detection Sub-Network. The decoder semantically projects the salient features of lower resolution from the encoders onto the pixel space having a higher resolution to achieve a semantic lesion pixel label [22, 53, 70]. The reduced feature maps (to attain spatial invariance) from the encoder often cause a loss in spatial resolution, bringing zigzag edge information, coarseness, checkerboard artifacts, and over- and under-segmentation in the segmented masks [33, 35, 53, 63, 70]. Although there are many approaches to alleviate these problems in the segmentation [2, 6, 33, 35, 53, 63, 70], there is still room for performance improvement. In our detection sub-network, the obtained outputs from two encoders are concatenated channel-wise for enlarging the depth representation of the feature map, which is named as a Fused Feature Map (FFM), where $FFM \in \mathcal{R}^{B \times H \times W \times 2D}$. We have applied skip connections, inspired by the UNet, to tackle the subsampling limitations. The $FFM \in \mathcal{R}^{B \times H \times W \times 2D}$ is an input to the decoder of our detection sub-network (see in Fig. 8). Unlike the earlier networks, we skip the features from two different encoders to recover the lost spatial information (see in Fig. 8). The channel-concatenation in each stage of decoder is presented as $[E_{1n} \# E_{2n} \# D_n]$, where E_{1n} , E_{2n} , D_n , and $\#$ respectively denote skipped feature maps from encoder-1 and encoder-2, decoder feature map (at n^{th} stage), and channel concatenation. E_{1n} , E_{2n} , and D_n are the same scaled feature maps and $n = 4, 3, \dots, 1$. Such a dual encoder skipped feature has enhanced depth information, which is likely to improve the segmentation accuracy by better retrieving the lost spatial information. Besides, we employ *batch normalization* [43] to overcome the internal covariate shift in the training phase. We also compact our network’s design, employing a DwSC [12] in place of standard convolution. We decrease the parameters by a factor of $(1/N + 1/K^2)$ for each convolution

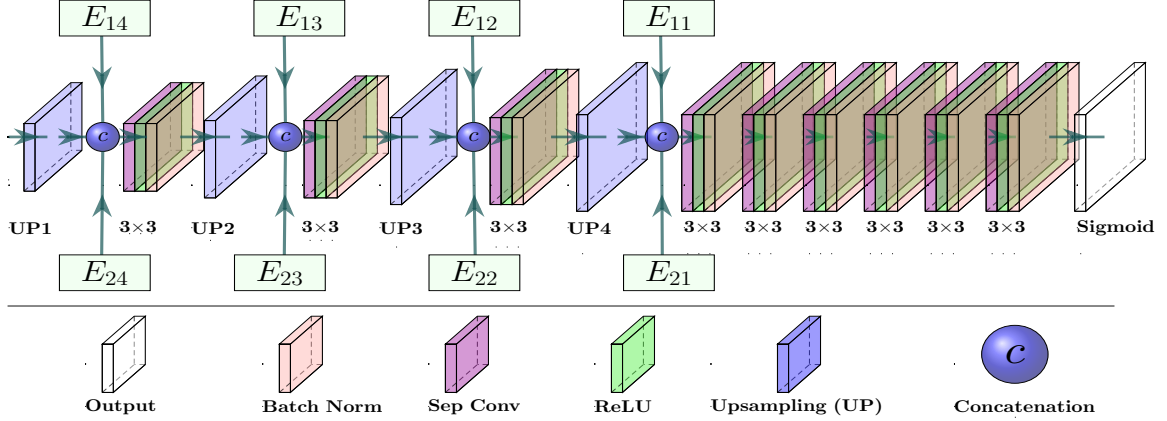


Figure 8: The decoder of the proposed detection sub-network for reconstructing a segmentation mask with the input resolution from the encoders’ low-resolution features.

in our Dermo-DOCTOR, where N and K respectively indicate the filter number and kernel size [34].

Recognition Sub-Network. Different feature maps from the encoder-1, encoder-2, and FFM are classified into desired categories applying the FCLs. We employ a Global Average Pooling (GAP) layer [52] before the FCL for vectorizing the 2D feature maps into a single long continuous linear vector, as it improves generalization and prevents overfitting [52]. Additionally, each FCL layer is followed by a *dropout* layer [78] as a regulariser, where we randomly set 50.0% neurons of the FC layer to zero during the training. However, the two different feature maps of two different encoders are utilized to recognize the Lesion Type (LT) separately using the two FCLs, termed as LT-1 and LT-2 (see in Fig. 5). Besides, the FFM also generates LT-3, as explicated in Fig. 5. Finally, the output probability ($O_{j=1,2}$) is the average of the LT-1, LT-2, and LT-3. The output ($O_{j=1,2}$) lies in N -dimensional space, where $O_1 \in \mathcal{R}^{N=2}$ and $O_2 \in \mathcal{R}^{N=3}$ respectively for the inputs I_1 or I_2 by applying the proposed preprocessing (either P_1 or P_2). It is noteworthy that the output lesion class ($O_{j=1,2}$) is obtained from the end-to-end training.

2.2. Designing of Web Application

The proposed web application named Dermo-DOCTOR, for the end-users, is depicted in Fig. 9. We utilize browser-supported languages such as Hypertext Markup Language

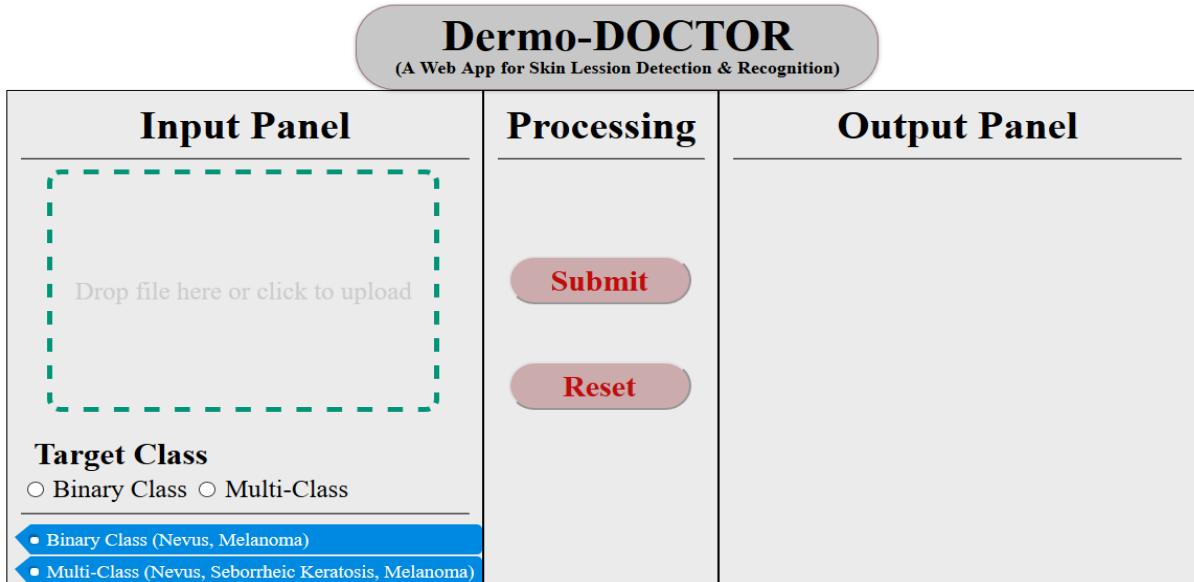


Figure 9: The dermo-DOCTOR prototype, where the user can select or drag a dermoscopic image (png, jpg, bmp, or jpeg) as an input. The desired number of output classes also can be selected in the input panel. The processing and output panels are dedicated to select the process types and display the recognized class with the probabilities.

(HTML), Cascading Style Sheets (CSS), and Javascript, *etc.* for developing the Dermo-DOCTOR application. A python web framework package, called Flask, is used for developing an application by deploying our proposed CNN-based detection and recognition models and their trained weights. We apply HTML and CSS to design a graphical user interface with three panels, such as an input panel, a processing panel, and an output panel (see in Fig. 9). The user can select the query image (drag-and-drop or direct upload) and the number of query classes (both binary and multi-class) in the input panel. Then, the user can also start the process or reset the selections in the processing panel. The return results from the host machine are displayed in the output panel.

2.3. Training Protocol

The encoder kernels are initialized with the pre-trained ImageNet weights, whereas the decoder kernels are initialized with the “he normal” distribution [39]. The Aspect Ratio (AS) distribution tells that most of the images in ISIC-2016 and ISIC-2017 datasets have an AS of 3 : 4. Therefore, we resize all the images to 192×256 pixels using the nearest-neighbor interpolation for the detection. Again, the AS distribution of both datasets’ extracted lesion ROIs reveals that most of the ROIs have an AS of 1 : 1. Hence, we again resize the lesion ROIs to 192×192 pixels using a nearest-neighbor interpolation for the recognition. Additionally, we have standardized and rescaled the training images to [0 1] for both detection and recognition. We employ Eq. 1 as a loss function and intersection over union as a metric for training the detection sub-network of the proposed Dermo-DOCTOR.

$$L(y, \hat{y}) = 1 - \frac{\sum_{i=1}^N y_i \times \hat{y}_i}{\sum_{i=1}^N y_i + \sum_{i=1}^N \hat{y}_i - \sum_{i=1}^N y_i \times \hat{y}_i} - \frac{1}{N} \sum_{i=1}^N [y_i \log \hat{y}_i + (1 - y_i) \log(1 - \hat{y}_i)], \quad (1)$$

where y and \hat{y} , N respectively denote the true and predicted label, the total pixel numbers. In Eq. 1, $\log \hat{y}_i$ and $\log(1 - \hat{y}_i)$ are the estimation of log-likelihood of pixel being lesion or not, respectively. The product of y and \hat{y} in Eq. 1 is the estimation of similarity (intersection) between true and predicted lesion masks. We employ categorical cross-entropy as a loss function and accuracy as a metric for training the recognition sub-network.

3. Results and Discussion

This section bestows different lesion detection results and subsequent recognition in Subsections 3.1 and 3.2, respectively. The segmented lesion masks are utilized for ROI extraction to classify and detect the bounding boxes around the lesions.

3.1. Results for Detection

Firstly, we exhibit the quantitative and qualitative segmentation results, applying the proposed Dermo-DOCTOR and two other well-known networks: the UNet and the FCN8s.

Secondly, we compare our outcomes with several state-of-the-art results utilizing the same datasets. To quantify the segmentation correctness, we use mean Recall (mRc), mean Specificity (mSp), and mean Intersection over Union (mIoU), which are defined in Eq. 2.

$$\begin{aligned}
 mRc &= \frac{1}{M \times N} \sum_{i=1}^N \sum_{j=1}^M \frac{TP_{ij}}{TP_{ij} + FN_{ij}}, \\
 mSp &= \frac{1}{M \times N} \sum_{i=1}^N \sum_{j=1}^M \frac{TN_{ij}}{TN_{ij} + FP_{ij}}, \\
 mIoU &= \frac{1}{M \times N} \sum_{i=1}^N \sum_{j=1}^M \frac{TP_{ij}}{TP_{ij} + FN_{ij} + FP_{ij}},
 \end{aligned} \tag{2}$$

where M and N denote the pixel and sample numbers, whereas TP , TN , FN , and FP indicate true positive (lesion as a lesion), true negative (background as a background), false negative (lesion as a background), and false positive (background as a lesion), respectively.

Table 1 confers the segmentation results of three methods on two separate datasets: the ISIC-2016 and the ISIC-2017. The mean overlapping between the actual and predicted masks

Table 1: Quantitative segmentation results on ISIC-2016 and ISIC-2017 test datasets using the Dermo-DOCTOR, UNet, and FCN8s. The winner metrics for the ISIC-2016 are presented in bold font, whereas they are underlined for the ISIC-2017.

Testing datasets	Models	Performance metrics		
		mRc	mSp	mIoU
ISIC-2016	Dermo-DOCTOR	0.92 ± 0.13	0.97 ± 0.07	0.85 ± 0.12
	UNet	0.86 ± 0.13	0.98 ± 0.04	0.83 ± 0.13
	FCN8s	0.84 ± 0.15	0.98 ± 0.05	0.80 ± 0.14
ISIC-2017	Dermo-DOCTOR	<u>0.86 ± 0.17</u>	<u>0.97 ± 0.07</u>	<u>0.80 ± 0.17</u>
	UNet	0.83 ± 0.21	0.97 ± 0.07	0.76 ± 0.21
	FCN8s	0.86 ± 0.18	0.93 ± 0.10	0.71 ± 0.17

are as high as 85.0% and 80.0% for the ISIC-2016 and ISIC-2017. The Dermo-DOCTOR mIoU beats nearby UNet by the margins of 2.0% and 4.0% accordingly for the ISIC-2016

and ISIC-2017 datasets. The mean type-I and type-II errors for ISIC-2016 of the Dermo-DOCTOR are 3.0 % and 8.0 %, respectively, outperforming the UNet by a margin of 6.0 % concerning the type-II error, while defeated by a margin of 1.0 % for type-I error. However, 1.0 % error in mSp is quite acceptable in segmentation as the lesion edge information will be preserved with less over-segmentation. Similarly, for ISIC-2017, the Dermo-DOCTOR exceeds UNet by a border of 3.0 % for type-II error, while they have similar type-I errors. For both the datasets, the FCN8s is a defeating method as it produces low metrics than the other two methods (see in Table 1). In contrast, the proposed Dermo-DOCTOR provides better-segmented masks, leading to better lesion detection and recognition.

Fig. 10 depicts several qualitative results from the proposed Dermo-DOCTOR, UNet, and FCN8s. The segmented lesions from FCN8s suffer from checkerboard artifact, providing zigzag lesion boundaries (see in Fig. 10). The possible cause of such poor results is that the low-resolution features across the high-resolution feature map are not constant due to the non-divisible upscaling factor, generating checkerboard artifacts in the lesion masks [33, 35]. However, the lesion masks from the UNet and Dermo-DOCTOR are blessed with smoother lesion boundaries, which are the image-based classifiers' salient features. The quantitative and qualitative results of the UNet point that it undergoes from the additional false-negative region, leading to under-segmentation. However, the proposed Dermo-DOCTOR achieves lower false-positive and false-negative regions relative to the other implementations. As in the proposed Dermo-DOCTOR, the dual encoders can learn more salient features compared to the single encoder in UNet and FCN8s, especially when training with a small dataset. Again, Fig. 11 illustrates the segmentation results of several challenging images on the ISIC-2016 and ISIC-2017 datasets. The lesion segmentation results in Fig. 11 describe that the segmented lesion masks are precise even the query images contain different artifacts (see in Fig. 2), and even the ROIs are tiny in size. Although the extracted ROIs have few false-positive regions (yellow color) with negligible false-negative regions (red color), it is not surprising for further lesion classification, as they preserve the lesion boundaries.

Table 2 exhibits lesion segmentation results from the proposed Dermo-DOCTOR and other state-of-the-art methods, trained and tested on the same ISIC datasets. The Dermo-

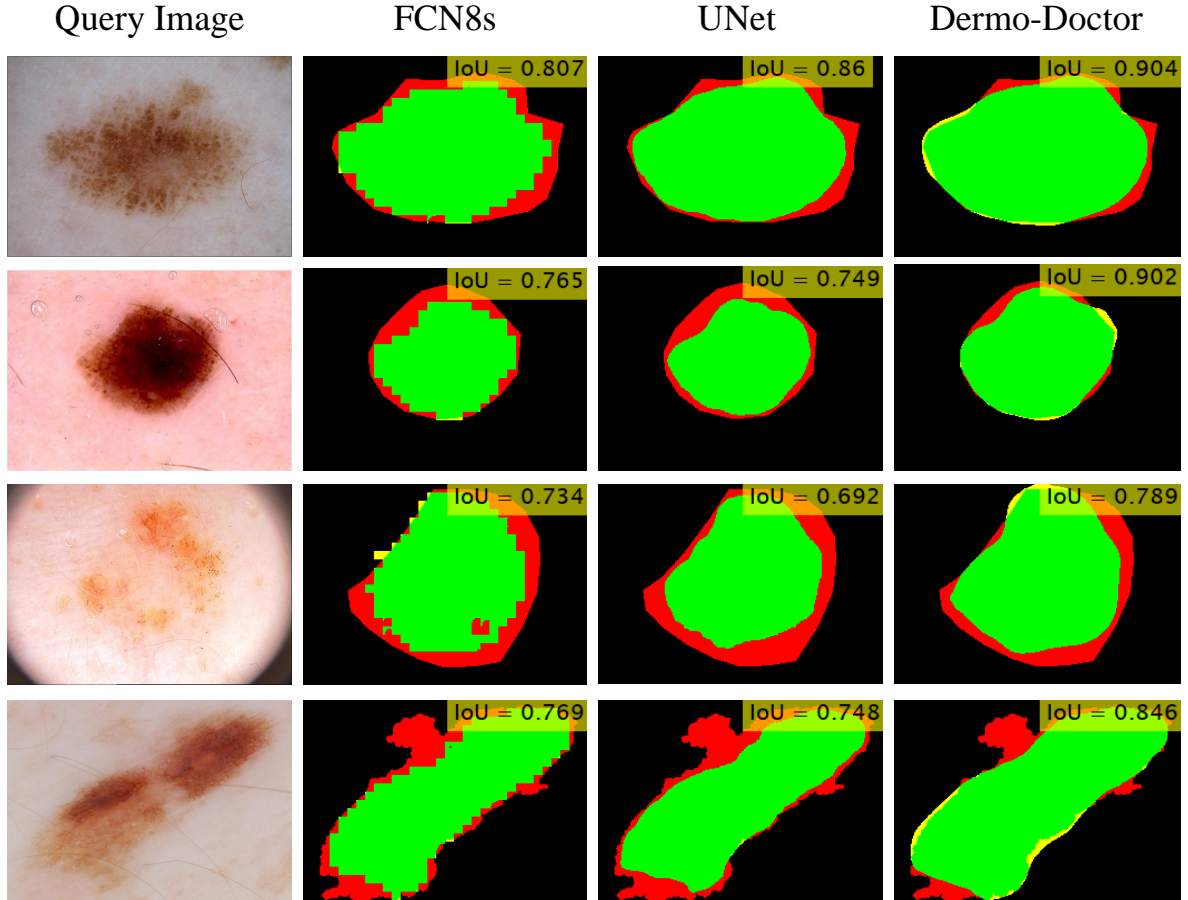


Figure 10: Qualitative segmentation results using the FCN8s, UNet, and Dermo-DOCTOR networks. Green, Red, and Yellow colors indicate the TP, FN, and FP regions, respectively. The top-right IoUs are given for quantitative evaluation.

DOCTOR generates the best segmentation results for three out of the six cases while performs as second-best for the remaining three cases. Our Dermo-DOCTOR outperforms the DCL-PSI [7] for ISIC-2016 by a margin of 1.0 % for mSp, whereas it has been lost by 1.0 % concerning mRc of DCL-PSI, while mIoU is constant for both methods. The current method (HRFB) of Xie et al. [85] has 5.0 % and 1.0 % less mRc and mSp, respectively, for ISIC-2016, while the mIoU is the same as our proposed method. It reveals that the proposed Dermo-DOCTOR has 5.0 % and 1.0 % less type-II and type-I errors, respectively, in the segmented lesion masks than HRFB. The Dermo-DOCTOR also defeats the other two methods, the FCN ensemble [90] and Fusion Structure [81], for all metrics and mSp for the ISIC-2016

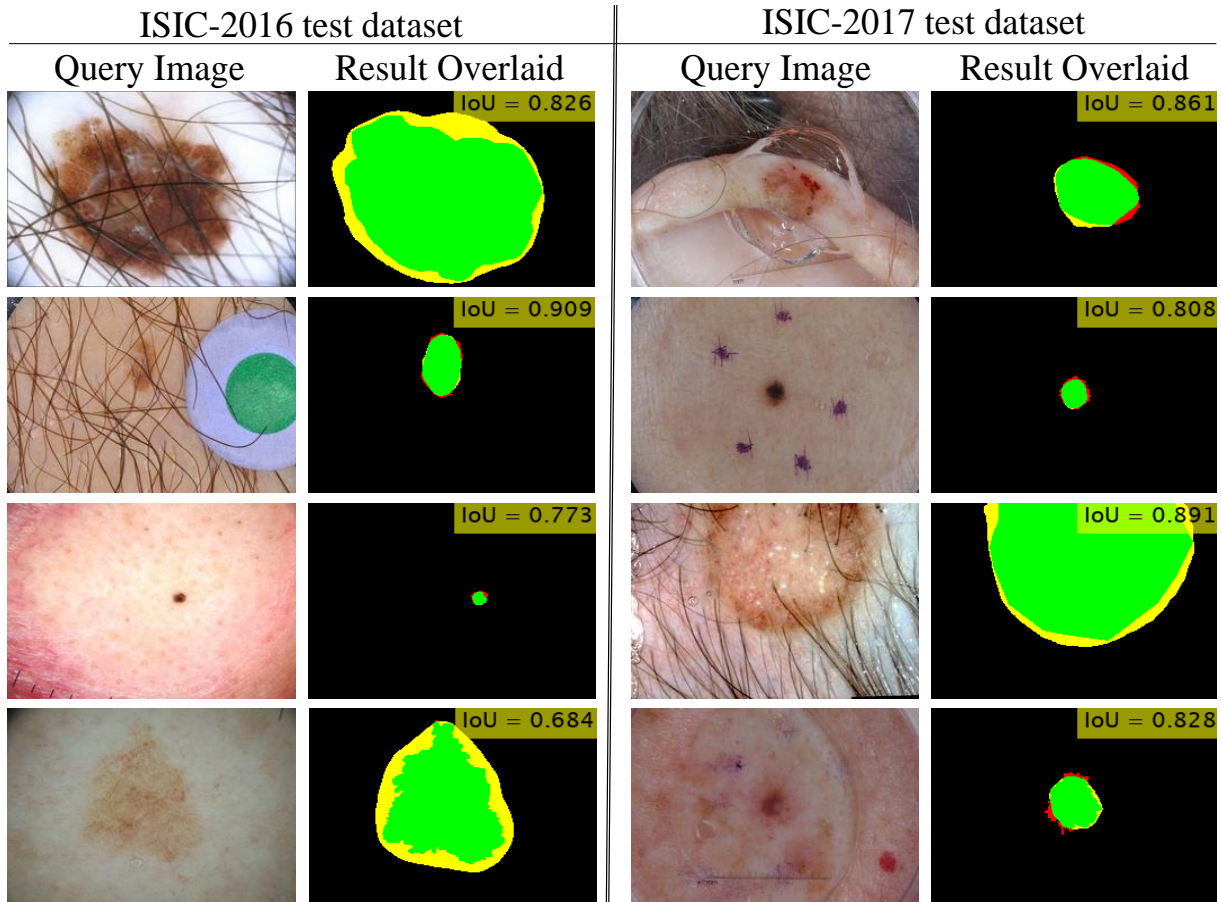


Figure 11: Qualitative segmentation results on two different test datasets employing our Dermo-DOCTOR, where the TP, FN, and FP regions are respectively denoted by the Green, Red, and Yellow colors. The top-right IoU exhibits quantitative validation.

dataset. Moreover, the methods in Table 2 for the ISIC-2017 dataset have been defeated by the proposed Dermo-DOCTOR for mIoU, where it beats the nearby HRFB and iFCN [65] by a margin of 2.0%. Regarding the mRc and mSp, the Dermo-DOCTOR has been lost by 1.0% by the methods in [35, 65, 85] (see in Table 2). Still, the Dermo-DOCTOR performs better as it has 2.0% more mIoU than the nearby methods [65, 85] for the ISIC-2107 dataset.

However, the above-discussions quantitatively and qualitatively demonstrate that the proposed Dermo-DOCTOR yields the most reliable skin lesion's ROIs, which proves its supremacy for lesion segmentation. Consequently, we will further utilize the proposed masks for lesion ROI extraction to perform the lesion recognition in the next subsection.

Table 2: Comparative lesion segmentation results for the proposed Dermo-DOCTOR and other state-of-the-art methods on both the ISIC-2016 and ISIC-2017 test datasets.

Segmentation Methods	ISIC-2016 test dataset			ISIC-2017 test dataset		
	mIoU	mRc	mSp	mIoU	mRc	mSp
FCN ensemble [90]	0.84	0.91	0.96	-	-	-
Fusion Structure [81]	0.85	0.92	0.96	-	-	-
DCL-PSI [7]	0.85	0.93	0.96	0.72	0.80	0.94
DSNet [35]	-	-	-	0.77	0.87	0.95
HRFB [85]	0.85	0.87	0.96	0.78	0.87	0.96
iFCN [65]	-	-	-	0.78	0.85	0.98
Proposed Dermo-DOCTOR (2020)	0.85	<u>0.92</u>	0.97	0.80	<u>0.86</u>	<u>0.97</u>

DCL-PSI: Deep Class-specific Learning with Probability based Step-wise Integration

HRFB: High-Resolution Feature Block

iFCN: improved Fully Convolutional Network

3.2. Results for Recognition

This subsection exhibits the quantitative and qualitative results for lesion recognition, applying the proposed Dermo-DOCTOR and two other implemented well-known networks: the ResNet-50 and the Xception. In the end, we compare our results with several state-of-the-art results for those datasets. We utilize recall, precision, and F1-score to quantify the recognition efficiency, where they respectively quantify the type-II error, the positive predictive values, and the harmonic mean of recall and precision for revealing the trade-off between them. Additionally, we also estimate the ROC curve and its corresponding AUC value to evaluate any randomly elected query image’s prediction probability.

Table 3 gives the lesion recognition results, showing the outcomes for three networks and two datasets. The weighted average of recalls for ResNet-50, Xception, and Dermo-DOCTOR have been respectively improved by the margins of 4.0%, 8.0%, and 7.0% for ISIC-2016, when we employ the preprocessing P_2 instead of baseline P_1 (see in Table 3). The highest possible recall (0.91) for ISIC-2016 is received from the proposed Dermo-DOCTOR classifier, applying the proposed preprocessing P_2 on the segmented masks from the pro-

Table 3: The recognition results from numerous comprehensive experiments on the ISIC-2016 and ISIC-2017 test datasets on three separate networks, highlighting the weighted average metrics’ highest values.

Test Dataset	Class-wise Metrics	ResNet-50		Xception		Dermo-DOCTOR		
		Preprocessing		Preprocessing		Preprocessing		
		P_1	P_2	P_1	P_2	P_1	P_2	
ISIC-2016	Recall	Nev	0.94	0.87	0.97	0.91	0.96	0.90
		Mel	0.45	0.93	0.25	0.92	0.37	0.95
		W. Avg.	0.84	0.88	0.83	0.91	0.84	0.91
	Precision	Nev	0.87	0.98	0.84	0.98	0.86	0.99
		Mel	0.64	0.63	0.70	0.71	0.68	0.70
		W. Avg.	0.83	0.91	0.81	0.93	0.83	0.93
	F1-score	Nev	0.90	0.92	0.90	0.94	0.91	0.94
		Mel	0.53	0.75	0.37	0.80	0.48	0.80
		W. Avg.	0.83	0.89	0.80	0.91	0.82	0.91
ISIC-2017	Recall	Nev	0.80	0.80	0.86	0.80	0.87	0.82
		SK	0.59	0.80	0.66	0.83	0.66	0.82
		Mel	0.45	0.59	0.42	0.53	0.50	0.62
		W. Avg.	0.70	0.76	0.74	0.75	0.77	0.78
	Precision	Nev	0.80	0.88	0.83	0.88	0.84	0.89
		SK	0.64	0.59	0.61	0.52	0.65	0.65
		Mel	0.43	0.56	0.52	0.62	0.58	0.57
		W. Avg.	0.70	0.78	0.74	0.77	0.76	0.79
	F1-score	Nev	0.80	0.84	0.85	0.84	0.85	0.85
		SK	0.61	0.68	0.63	0.64	0.65	0.73
		Mel	0.44	0.57	0.46	0.57	0.53	0.59
		W. Avg.	0.70	0.76	0.74	0.76	0.76	0.78

P_1 : Segmentation; P_2 : Segmentation+Rebalancing+Augmentation; W. Avg.: Weighted Average

posed Dermo-DOCTOR segmentor. The rebalancing and augmentation, along with the segmentation, in preprocessing P_2 reduces the FN-rates (63.0% to 5.0%) of Mel class. It also decreases the FP-rates (32.0% to 30.0%) for the same class while applying our proposed Dermo-DOCTOR. Such reductions, in FN- and FP-rates, are praiseworthy of our proposed preprocessing P_2 and Dermo-DOCTOR comparing the baseline classifiers (ResNet-50

and Xception) and preprocessing P_1 . Likewise, the weighted average of precision and F1-score on ISIC-2016 are also respectively improved by 10.0 % and 9.0 % for the preprocessing P_2 . Remarkably, the harmonic mean of recall and precision for the Mel class of ISIC-2016 has significantly strengthened by a margin of 32.0 % with preprocessing (P_2) and Dermo-DOCTOR. However, comparing all the experiments on the ISIC-2016, the proposed P_2 and Dermo-DOCTOR are the best preprocessing and classifier having a type-II error of 9.0 % and positive predictive value of 93.0 %. Table 3 also notes that the weighted average of recall, precision, and F1-score have the respective maximum values of 0.78, 0.79, and 0.78, for the preprocessing P_2 and proposed Dermo-DOCTOR on the ISIC-2017. The recall of SK and Mel classes in the ISIC-2017 dataset, applying the proposed Dermo-DOCTOR and preprocessing P_2 , have respectively updated by the margins of 16.0 % and 12.0 %. In comparison, it decreases by 1.0 % for the Nev class, which is acceptable in the medical diagnostic system (as the positive class is significantly improved). A margin of 5.0 % has raised the Nev class’s positive predictive value, whereas it is closer or equal for the other two classes for the proposed Dermo-DOCTOR with P_2 . However, comparing all the experiments on the ISIC-2017, the proposed P_2 and Dermo-DOCTOR are the best preprocessing and classifier, with a type-II error of 22.0 % and positive predictive value of 79.0 %.

The experimental lesion categorization results on ISIC-2016 and ISIC-2017 datasets demonstrate that the two-classes’ (ISIC-2016) recognition performance is better than the three-classes (ISIC-2017). The addition of SK class in ISIC-2017 reduces the weighted average recall, precision, and F1-score by the margins of 13.0 %, 14.0 %, and 13.0 %, respectively. The higher similarity of SK with Nev and Mel classes is the possibility of such reduced ISIC-2017 test results. Noticeably, more classes tend to bring complications to the classifiers, especially when the training has fewer examples and inter-class similarities. The joining of different heterogeneous samples to each class can enhance the categorization results in ISIC-2017.

The further analysis of different classifiers and preprocessing have presented in the ROC curves in Fig. 12, showing the highest possible AUC as 0.98 and 0.91 respectively for ISIC-2016 and ISIC-2017. The rebalancing and augmentation employment with segmentation

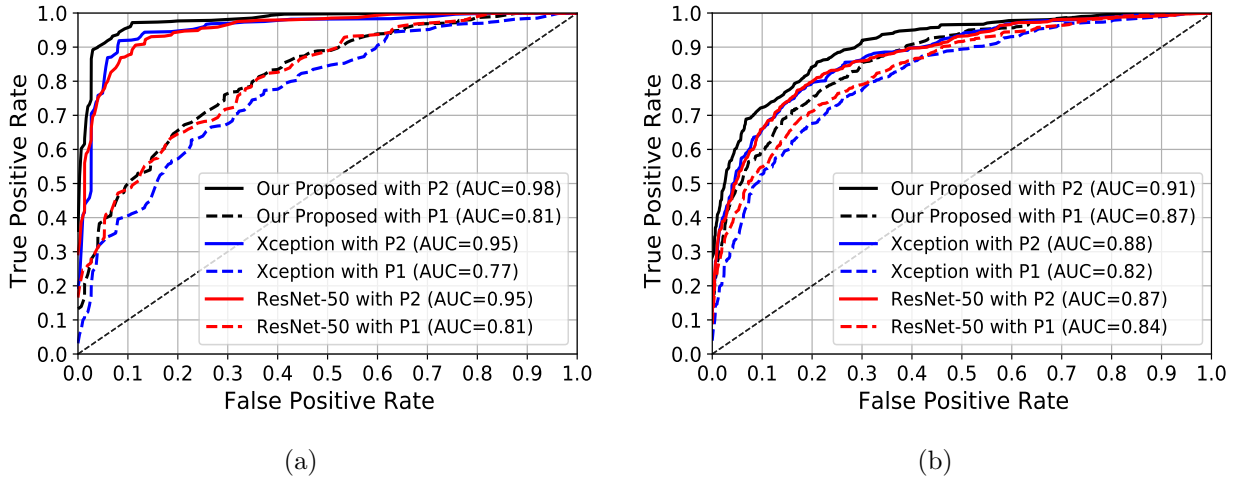


Figure 12: The ROC curves ((a) for ISIC-2016 and (b) for ISIC-2017) of skin lesion recognition, where we have plotted the ROC for the proposed Dermo-DOCTOR and implemented ResNet-50 and Xception with two different preprocessing (P_1 and P_2).

(P_2) heightens AUC for both ISIC-2016 and ISIC-2017 datasets of all classifiers. The Dermo-DOCTOR with P_2 has beaten the baseline Xception and ResNet-50 respectively by 3.0% and 3.0% in terms of AUC for the ISIC-2016 dataset. Whereas it surpasses them by the margins of 3.0% and 4.0% for AUC for the ISIC-2017 dataset. However, the earlier discussions for the lesion recognition on ISIC-2016 and ISIC-2017 test datasets expose the supremacy of the proposed Dermo-DOCTOR and preprocessing P_2 .

The detailed class-wise performances of the lesion recognition by the proposed Dermo-DOCTOR and preprocessing P_2 are exhibited in Table 4. The ISIC-2016’s confusion matrix in Table 4 (left) shows that among 304-Nev samples correctly recognized samples are 273 (89.80%), whereas barely 31 (10.20%)-Nev samples are recognized as Mel (as FP). It also reveals that among 75-Mel samples, rightly recognized samples are 71 (94.67%), whereas only 4 (5.33%)-Mel samples are improperly recognized as Nev (as FN). Again, the ISIC-2017’s confusion matrix (see in Table 4 (right)) demonstrates that 81.68%-Nev samples are correctly recognized as Nev class, while 18.32%-Nev samples are wrongly recognized to other classes as FP (5.85% as SK and 12.47% as Mel). Similarly, 17.78% and 38.46% samples of the SK- and Mel-classes belong to FP and FN, respectively. Although the 38.46% of

Table 4: The confusion matrix for the ISIC-2016 with 379 samples (left) and ISIC-2016 with 600 samples (right) test datasets, employing the proposed Dermo-DOCTOR and preprocessing P_2

			Actual					
		Nev	Mel					
Predicted	Nev	273 89.80 %	4 5.33 %	Predicted	Nev	321 81.68 %	10 11.11 %	28 23.93 %
	Mel	31 10.20 %	71 94.67 %		SK	23 5.85 %	74 82.22 %	17 14.53 %
				Mel	49 12.47 %	6 6.67 %	72 61.54 %	

the positive samples (Mel) are improperly recognized, it is still better than the baseline 58.0% errors in the baseline (Xception with preprocessing P_1). Fig. 13 bestows qualitative results from the proposed Dermo-DOCTOR classifier and preprocessing P_2 for the lesion recognition into different, either two classes or three classes. For concurrent detection and recognition, we utilize the segmented masks and categorized class for contouring the lesions (green color) and label annotation on the image to help the dermatologists for further assessment (see in Fig. 13). More concurrent results for all the test images are available on YouTube (ISIC-2016³ and ISIC-2017⁴). However, the results in Fig. 13 illustrate a few challenging images, where we show some wrongly recognized images. Those qualitative results depict that the detection and recognition are precise even the query test images contain different artifacts (see in Fig. 2). Although the Dermo-DOCTOR incorrectly predicts some images, they visually seem like a predicted class.

Table 5 describes the comparison of the results of our Dermo-DOCTOR and other methods, which were trained and tested on the same ISIC datasets. The proposed Dermo-DOCTOR produces the best recognition for two out of the six cases while performing second-best with the winning methods on the other four cases (see in Table 5).

³ISIC-2016 (Detection & Recognition): https://bit.ly/Dermo-DOCTOR_ISIC_16

⁴ISIC-2017 (Detection & Recognition): https://bit.ly/Dermo-DOCTOR_ISIC_17

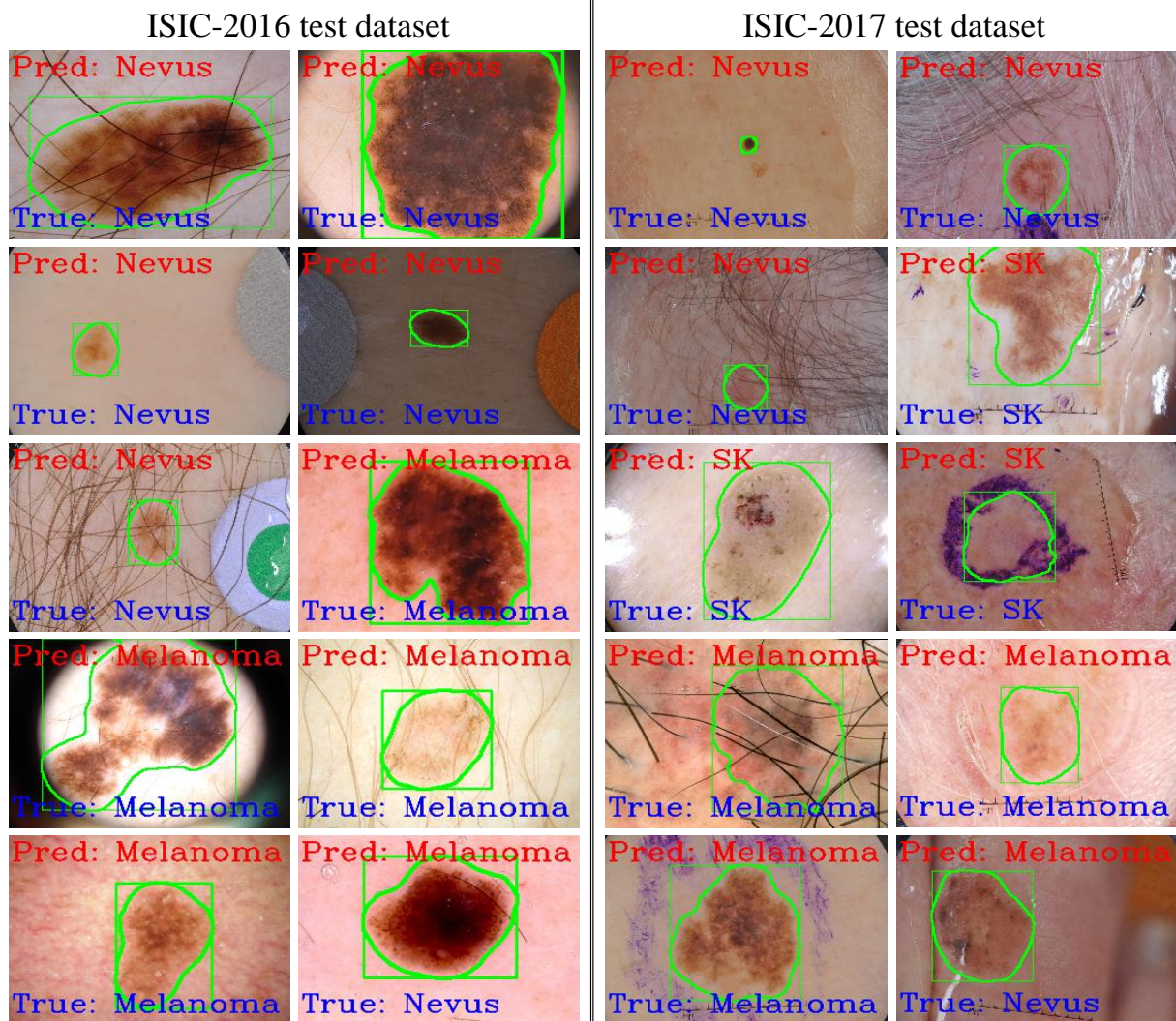


Figure 13: Example of several qualitative classification results of the challenging images of the ISIC-2016 and ISIC-2017 test datasets using the Dermo-DOCTOR, where the recognition has accomplished using the segmented ROIs (green color) from the Dermo-DOCTOR.

Comparison of ISIC-2016. The proposed network produces the best results for the AUC by beating the state-of-the-art of Yu et al. [89] with a 12.0% border. Concerning the type-II errors, Dermo-DOCTOR is behind the state-of-the-art (FPRPN) of Song et al. [77] by a border of 8.0%, but the Dermo-DOCTOR outperforms it by a 11.0% border for the positive predictive value. However, Dermo-DOCTOR beats the FPRPN by a 1.5% perimeter in terms of balanced accuracy. Whereas Dermo-DOCTOR also exceeds the FPRPN by a

Table 5: The state-of-the-art comparison with proposed Dermo-DOCTOR, which had trained, validated, and tested on the ISIC-2016 and ISIC-2017 datasets.

Classification Methods	ISIC-2016 test dataset			ISIC-2017 test dataset		
	Recall	Precision	AUC	Recall	Precision	AUC
ResNet-50 [10]	0.56	0.71	0.85	-	-	-
GR [74]	-	-	-	0.15	-	0.91
ARLCNN [91]	-	-	-	0.77	-	0.92
IR [3]	0.82	-	0.77	0.76	-	-
FPRPN [77]	0.99	<u>0.82</u>	0.81	0.98	0.82	0.79
MFA [89]	0.60	0.69	<u>0.86</u>	-	0.72	0.90
Proposed Dermo-DOCTOR (2020)	<u>0.91</u>	0.93	0.98	<u>0.78</u>	<u>0.79</u>	<u>0.91</u>

GR: Gabor Wavelet-based CNN [74]

ARLCNN: Attention Residual Learning CNN (ResNet-14 & ResNet-50) [92]

IR: Inception-ResNet-V2 (ISIC-2016), ResNet-50 (ISIC-2017,ISIC-2018) [3]

FPRPN: Feature Pyramid Network (FPN) and Region Proposal Network (RPN) [77]

MFA: Multi-network based feature aggregation [89]

17.0 % margin for AUC.

Comparison of ISIC-2017. The Dermo-DOCTOR serves as the second-best results concerning all the metrics, where it beats the state-of-the-art FPRPN [77] with a margin of 12.0 % for AUC, although FPRPN has defeated it for balanced accuracy. The proposed Dermo-DOCTOR has defeated ARLCNN [91] by a 1.0 % border concerning the recall, but ARLCNN wins by a 1.0 % margin in AUC. However, the proposed Dermo-DOCTOR produces the second-highest results for recall by beating the third-best ARLCNN [91] with a margin of 1.0 %. For precision, it performs so by vanquishing third-best MFA [89] with a border of 7.0 %, and for AUC by beating third-best MFA with a margin of 1.0 %.

3.3. Applications

Fig. 14 illustrates the prototype of the developed web application deploying our Dermo-DOCTOR, which runs in a web browser at “http://127.0.0.1:5000/” by accessing the CNN environments of the local machine. The app takes a dermoscopic image (png, jpg, bmp,

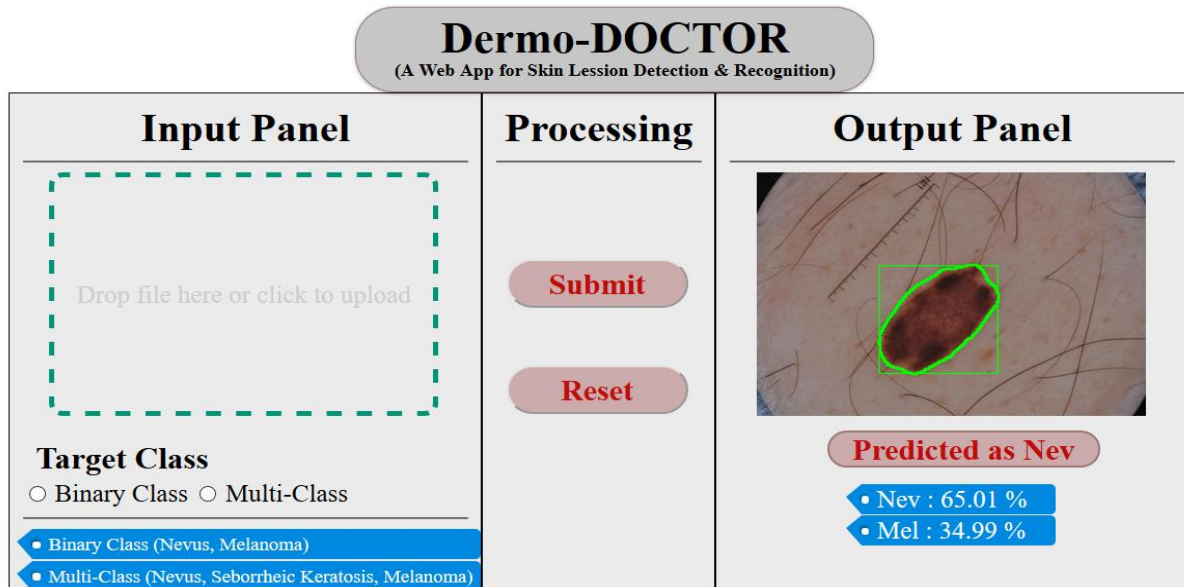


Figure 14: Our designed web application to detect and recognize skin lesions simultaneously. Dermatologists can utilize this application by selecting or dragging the image as an input. The app will confer the lesion detection and recognition results for either binary class or multi-classes.

or jpeg) as an input, displaying the user’s diagnosis result as soon as the back-end model analyzes a given image. The recognized class with its probability is displayed in the output panel, highlighting the lesion ROI by a green color bounding box. Therefore, it helps the dermatologists focus on that detected area for cross-checking the predicted class. A real-time utilization of the Dermo-DOCTOR has been uploaded to YouTube⁵, which confers less time-latency of getting results. The reason for that is the app sends images to the host and receives the host’s results through the internet and the time for prediction in the host (higher traffic in the host will increase the latency). However, the dedicated machine with GPU can alleviate this time-latency limitation. We have tested the app on our local machine and could not make it public due to resource limitations.

⁵Dermo-DOCTOR App: https://bit.ly/Dermo-DOCTOR_App

4. Conclusion

Despite the present colossal challenges due to high visual and intra-class variability, inter-class similarity, and the presence of different artifacts, automated skin lesion detection and recognition are incredibly crucial. However, this article proposed and developed an automated CNN-based lesion detection and recognition network, integrating ROI extraction by segmentation, image augmentations, and class rebalancing. Our experimental results demonstrated that the proposed Dermo-DOCTOR could detect and recognize the lesion more accurately as we concatenated features from two different encoders. Such a concatenation provides more prominent and discriminating feature maps of the skin lesions comparing a single encoder. The segmented lesions rather than the whole images can provide more salient and representative features from the CNNs, leading to improved lesion recognition. Moreover, the rebalanced class distribution attained better performance of the recognition as compared to the imbalanced distribution. Additionally, the augmentation led the CNN-based classifier to be more generic as CNNs can learn from diverse training samples. Thus, it achieved state-of-the-art performance to detect and recognize the lesions from two different test datasets, such as ISIC-2016 and ISIC-2017. We will further explore and investigate the effects of improved segmentation and weighting of the underrepresented classes in the future. The deployment of our framework to a web application precisely detected and recognized the lesions concurrently. The developed web application will be improved, making it more user-friendly for dermatologists and deploying it to the google cloud platform for clinical applications.

Author Contributions

M. K. Hasan: Conceptualization, Methodology, Software, Formal analysis, Investigation, Writing- Review & Editing, Supervision; **S. Roy:** Validation, Data Curation, Writing- Original Draft; **C. Mondal:** Validation, Data Curation, Writing- Original Draft; **M. A. Alam:** Conceptualization, Data Curation; **M. T. E. Elahi:** Validation, Writing- Original Draft; **A. Dutta:** Validation, Writing- Original Draft; **S. M. T. U. Raju:** Software; **M.**

T. Jawad: Validation, Writing- Review & Editing; **M. Ahmad:** Supervision.

Acknowledgements

None. No funding to declare.

Conflict of Interest

All authors have no conflict of interest to publish this research.

References

- [1] Acharya, U.R., Molinari, F., Sree, S.V., Chattopadhyay, S., Ng, K.H., Suri, J.S., 2012. Automated diagnosis of epileptic eeg using entropies. *Biomedical Signal Processing and Control* 7, 401–408.
- [2] Al-Masni, M.A., Al-antari, M.A., Choi, M.T., Han, S.M., Kim, T.S., 2018. Skin lesion segmentation in dermoscopy images via deep full resolution convolutional networks. *Computer methods and programs in biomedicine* 162, 221–231.
- [3] Al-Masni, M.A., Kim, D.H., Kim, T.S., 2020. Multiple skin lesions diagnostics via integrated deep convolutional networks for segmentation and classification. *Computer Methods and Programs in Biomedicine* 190, 105351.
- [4] Al Nazi, Z., Abir, T.A., 2020. Automatic skin lesion segmentation and melanoma detection: Transfer learning approach with u-net and dcnn-svm, in: *Proceedings of International Joint Conference on Computational Intelligence*, Springer. pp. 371–381.
- [5] Amin, J., Sharif, A., Gul, N., Anjum, M.A., Nisar, M.W., Azam, F., Bukhari, S.A.C., 2020. Integrated design of deep features fusion for localization and classification of skin cancer. *Pattern Recognition Letters* 131, 63–70.
- [6] Badrinarayanan, V., Kendall, A., Cipolla, R., 2017. SegNet: A deep convolutional encoder-decoder architecture for image segmentation. *IEEE transactions on pattern analysis and machine intelligence* 39, 2481–2495.
- [7] Bi, L., Kim, J., Ahn, E., Kumar, A., Feng, D., Fulham, M., 2019. Step-wise integration of deep class-specific learning for dermoscopic image segmentation. *Pattern recognition* 85, 78–89.
- [8] Bi, L., Kim, J., Ahn, E., Kumar, A., Fulham, M., Feng, D., 2017. Dermoscopic image segmentation via multistage fully convolutional networks. *IEEE Transactions on Biomedical Engineering* 64, 2065–2074.
- [9] Bray, F., Ferlay, J., Soerjomataram, I., Siegel, R.L., Torre, L.A., Jemal, A., 2018. Global cancer statistics 2018: Globocan estimates of incidence and mortality worldwide for 36 cancers in 185 countries. *CA: a cancer journal for clinicians* 68, 394–424.

- [10] Brinker, T.J., Hekler, A., Enk, A.H., von Kalle, C., 2019. Enhanced classifier training to improve precision of a convolutional neural network to identify images of skin lesions. *PloS one* 14.
- [11] Cheng, Y., Swamisai, R., Umbaugh, S.E., Moss, R.H., Stoecker, W.V., Teegala, S., Srinivasan, S.K., 2008. Skin lesion classification using relative color features. *Skin Research and Technology* 14, 53–64.
- [12] Chollet, F., 2017. Xception: Deep learning with depthwise separable convolutions, in: *Proceedings of the IEEE conference on computer vision and pattern recognition*, pp. 1251–1258.
- [13] Codella, N.C., Gutman, D., Celebi, M.E., Helba, B., Marchetti, M.A., Dusza, S.W., Kalloo, A., Liopyris, K., Mishra, N., Kittler, H., et al., 2018. Skin lesion analysis toward melanoma detection: A challenge at the 2017 international symposium on biomedical imaging (isbi), hosted by the international skin imaging collaboration (isic), in: *2018 IEEE 15th International Symposium on Biomedical Imaging (ISBI 2018)*, IEEE. pp. 168–172.
- [14] Deng, J., Dong, W., Socher, R., Li, L.J., Li, K., Fei-Fei, L., 2009. Imagenet: A large-scale hierarchical image database, in: *2009 IEEE conference on computer vision and pattern recognition, Ieee*. pp. 248–255.
- [15] Dennis Schmid, 2018. *Number of dermatologists in selected European countries in 2015*. <https://tinyurl.com/y59xoc7n> [Accessed: 4 Sept 2020].
- [16] Department of Health (Commonwealth of Australia), 2017. *Dermatology 2016 Factsheet*. <https://tinyurl.com/y3z39b9r> [Accessed: 15 Jun 2020].
- [17] Dolz, J., Desrosiers, C., Wang, L., Yuan, J., Shen, D., Ayed, I.B., 2020. Deep cnn ensembles and suggestive annotations for infant brain mri segmentation. *Computerized Medical Imaging and Graphics* 79, 101660.
- [18] Estava, A., Kuprel, B., Novoa, R., et al., 2017. Dermatologist level classification of skin cancer with deep neural networks [j]. *Nature* 542, 115.
- [19] Everingham, M., Van Gool, L., Williams, C.K., Winn, J., Zisserman, A., 2010. The pascal visual object classes (voc) challenge. *International journal of computer vision* 88, 303–338.
- [20] Fujisawa, Y., Inoue, S., Nakamura, Y., 2019. The possibility of deep learning-based, computer-aided skin tumor classifiers. *Frontiers in Medicine* 6, 191.
- [21] Furey, T.S., Cristianini, N., Duffy, N., Bednarski, D.W., Schummer, M., Haussler, D., 2000. Support vector machine classification and validation of cancer tissue samples using microarray expression data. *Bioinformatics* 16, 906–914.
- [22] Garcia-Garcia, A., Orts-Escolano, S., Oprea, S., Villena-Martinez, V., Martinez-Gonzalez, P., Garcia-Rodriguez, J., 2018. A survey on deep learning techniques for image and video semantic segmentation. *Applied Soft Computing* 70, 41–65.
- [23] Ge, Z., Demyanov, S., Chakravorty, R., Bowling, A., Garnavi, R., 2017. Skin disease recognition using

- deep saliency features and multimodal learning of dermoscopy and clinical images, in: International Conference on Medical Image Computing and Computer-Assisted Intervention, Springer. pp. 250–258.
- [24] Gessert, N., Nielsen, M., Shaikh, M., Werner, R., Schlaefel, A., 2020. Skin lesion classification using ensembles of multi-resolution efficientnets with meta data. *MethodsX* , 100864.
- [25] Ghadiyaram, D., Bovik, A.C., 2017. Perceptual quality prediction on authentically distorted images using a bag of features approach. *Journal of vision* 17, 32–32.
- [26] Glazer, A.M., Rigel, D.S., 2017. Analysis of trends in geographic distribution of us dermatology workforce density. *JAMA dermatology* 153, 472–473.
- [27] Goyal, M., Oakley, A., Bansal, P., Dancey, D., Yap, M.H., 2019. Skin lesion segmentation in dermoscopic images with ensemble deep learning methods. *IEEE Access* .
- [28] Guo, Y., Liu, Y., Oerlemans, A., Lao, S., Wu, S., Lew, M.S., 2016. Deep learning for visual understanding: A review. *Neurocomputing* 187, 27–48.
- [29] Gutman, D., Codella, N.C., Celebi, E., Helba, B., Marchetti, M., Mishra, N., Halpern, A., 2016. Skin lesion analysis toward melanoma detection: A challenge at the international symposium on biomedical imaging (isbi) 2016, hosted by the international skin imaging collaboration (isic). arXiv:1605.01397 .
- [30] Ha, Q., Liu, B., Liu, F., 2020. Identifying melanoma images using efficientnet ensemble: Winning solution to the siim-isic melanoma classification challenge. arXiv preprint arXiv:2010.05351 .
- [31] Hameed, N., Shabut, A.M., Ghosh, M.K., Hossain, M., 2020. Multi-class multi-level classification algorithm for skin lesions classification using machine learning techniques. *Expert Systems with Applications* 141, 112961.
- [32] Harangi, B., 2018. Skin lesion classification with ensembles of deep convolutional neural networks. *Journal of biomedical informatics* 86, 25–32.
- [33] Hasan, M.K., Alam, M.A., Elahi, M.T.E., Roy, S., Martí, R., 2021a. Drnet: Segmentation and localization of optic disc and fovea from diabetic retinopathy image. *Artificial Intelligence in Medicine* 111, 102001.
- [34] Hasan, M.K., Calvet, L., Rabbani, N., Bartoli, A., 2021b. Detection, segmentation, and 3d pose estimation of surgical tools using convolutional neural networks and algebraic geometry. *Medical Image Analysis* , 101994.
- [35] Hasan, M.K., Dahal, L., Samarakoon, P.N., Tushar, F.I., Martí, R., 2020. Dsnet: Automatic dermoscopic skin lesion segmentation. *Computers in Biology and Medicine* , 103738.
- [36] Hawas, A.R., Guo, Y., Du, C., Polat, K., Ashour, A.S., 2020. Oce-ngc: A neutrosophic graph cut algorithm using optimized clustering estimation algorithm for dermoscopic skin lesion segmentation. *Applied Soft Computing* 86, 105931.
- [37] He, H., Garcia, E.A., 2009. Learning from imbalanced data. *IEEE Transactions on knowledge and data*

- engineering 21, 1263–1284.
- [38] He, K., Gkioxari, G., Dollár, P., Girshick, R., 2017. Mask r-cnn, in: Proceedings of the IEEE international conference on computer vision, pp. 2961–2969.
 - [39] He, K., Zhang, X., Ren, S., Sun, J., 2015. Delving deep into rectifiers: Surpassing human-level performance on imagenet classification, in: Proceedings of the IEEE international conference on computer vision, pp. 1026–1034.
 - [40] He, K., Zhang, X., Ren, S., Sun, J., 2016. Deep residual learning for image recognition, in: Proceedings of the IEEE conference on computer vision and pattern recognition, pp. 770–778.
 - [41] Hu, J., Shen, L., Sun, G., 2018. Squeeze-and-excitation networks, in: Proceedings of the IEEE conference on computer vision and pattern recognition, pp. 7132–7141.
 - [42] Huang, G., Liu, Z., Van Der Maaten, L., Weinberger, K.Q., 2017. Densely connected convolutional networks, in: Proceedings of the IEEE conference on computer vision and pattern recognition, pp. 4700–4708.
 - [43] Ioffe, S., Szegedyet, C., 2015. Batch Normalization: accelerating deep network training by reducing internal covariate shift. arXiv:1502.03167 .
 - [44] ISIC, 2018. *ISIC Archive*. <https://tinyurl.com/11hgg83u> [Accessed: 09 May 2020].
 - [45] Jahanifar, M., Tajeddin, N.Z., Asl, B.M., Gooya, A., 2018. Supervised saliency map driven segmentation of lesions in dermoscopic images. *IEEE journal of biomedical and health informatics* 23, 509–518.
 - [46] Kermany, D.S., Goldbaum, M., Cai, W., Valentim, C.C., Liang, H., Baxter, S.L., McKeown, A., Yang, G., Wu, X., Yan, F., et al., 2018. Identifying medical diagnoses and treatable diseases by image-based deep learning. *Cell* 172, 1122–1131.
 - [47] Khan, M.A., Sharif, M., Akram, T., Bukhari, S.A.C., Nayak, R.S., 2020. Developed newton-raphson based deep features selection framework for skin lesion recognition. *Pattern Recognition Letters* 129, 293–303.
 - [48] Krizhevsky, A., Sutskever, I., Hinton, G.E., 2012. Imagenet classification with deep convolutional neural networks, in: *Advances in neural information processing systems*, pp. 1097–1105.
 - [49] Kumar, A., Kim, J., Lyndon, D., Fulham, M., Feng, D., 2016. An ensemble of fine-tuned convolutional neural networks for medical image classification. *IEEE journal of biomedical and health informatics* 21, 31–40.
 - [50] Lattoofi, N.F., Al-sharuee, I.F., Kamil, M.Y., Obaid, A.H., Mahidi, A.A., Omar, A.A., et al., 2019. Melanoma skin cancer detection based on abcd rule, in: *2019 First International Conference of Computer and Applied Sciences (CAS)*, IEEE. pp. 154–157.
 - [51] Lee, Y.C., Jung, S.H., Won, H.H., 2018. Wonderm: Skin lesion classification with fine-tuned neural networks. arXiv preprint arXiv:1808.03426 .

- [52] Lin, M., Chen, Q., Yan, S., 2013. Network in network. arXiv:1312.4400 .
- [53] Long, J., Shelhamer, E., Darrell, T., 2015. Fully convolutional networks for semantic segmentation, in: Proceedings of the IEEE conference on computer vision and pattern recognition, pp. 3431–3440.
- [54] Lowe, D.G., 2004. Distinctive image features from scale-invariant keypoints. *International journal of computer vision* 60, 91–110.
- [55] Maćkiewicz, A., Ratajczak, W., 1993. Principal components analysis (pca). *Computers & Geosciences* 19, 303–342.
- [56] Maglogiannis, I., Doukas, C.N., 2009. Overview of advanced computer vision systems for skin lesions characterization. *IEEE transactions on information technology in biomedicine* 13, 721–733.
- [57] Mahbod, A., Schaefer, G., Ellinger, I., Ecker, R., Pitiot, A., Wang, C., 2019. Fusing fine-tuned deep features for skin lesion classification. *Computerized Medical Imaging and Graphics* 71, 19–29.
- [58] Mahbod, A., Schaefer, G., Wang, C., Dorffner, G., Ecker, R., Ellinger, I., 2020. Transfer learning using a multi-scale and multi-network ensemble for skin lesion classification. *Computer methods and programs in biomedicine* 193, 105475.
- [59] Moitra, D., Mandal, R.K., 2020. Prediction of non-small cell lung cancer histology by a deep ensemble of convolutional and bidirectional recurrent neural network. *Journal of Digital Imaging* , 1–8.
- [60] Mporas, I., Perikos, I., Paraskevas, M., 2020. Color models for skin lesion classification from dermatoscopic images, in: *Advances in Integrations of Intelligent Methods*. Springer, pp. 85–98.
- [61] Nachbar, F., Stolz, W., Merkle, T., Cagnetta, A.B., Vogt, T., Landthaler, M., Bilek, P., Braun-Falco, O., Plewig, G., 1994. The abcd rule of dermatoscopy: high prospective value in the diagnosis of doubtful melanocytic skin lesions. *Journal of the American Academy of Dermatology* 30, 551–559.
- [62] Navarro, F., Escudero-Viñolo, M., Bescós, J., 2018. Accurate segmentation and registration of skin lesion images to evaluate lesion change. *IEEE journal of biomedical and health informatics* 23, 501–508.
- [63] Odena, A., Dumoulin, V., Olah, C., 2016. Deconvolution and checkerboard artifacts. *Distill* 1, e3.
- [64] Oliveira, R.B., Papa, J.P., Pereira, A.S., Tavares, J.M.R., 2018. Computational methods for pigmented skin lesion classification in images: review and future trends. *Neural Computing and Applications* 29, 613–636.
- [65] Öztürk, Ş., Özkaya, U., 2020. Skin lesion segmentation with improved convolutional neural network. *Journal of digital imaging* .
- [66] Pacheco, A.G., Ali, A.R., Trappenberg, T., 2019. Skin cancer detection based on deep learning and entropy to detect outlier samples. arXiv preprint arXiv:1909.04525 .
- [67] Pour, M.P., Seker, H., 2020. Transform domain representation-driven convolutional neural networks for skin lesion segmentation. *Expert Systems with Applications* 144, 113129.

- [68] Qin, Z., Liu, Z., Zhu, P., Xue, Y., 2020. A gan-based image synthesis method for skin lesion classification. *Computer Methods and Programs in Biomedicine* , 105568.
- [69] Rajpurkar, P., Irvin, J., Zhu, K., Yang, B., Mehta, H., Duan, T., Ding, D., Bagul, A., Langlotz, C., Shpanskaya, K., et al., 2017. Chexnet: Radiologist-level pneumonia detection on chest x-rays with deep learning. *arXiv:1711.05225* .
- [70] Ronneberger, O., Fischer, P., Brox, T., 2015. U-net: Convolutional networks for biomedical image segmentation, in: *International Conference on Medical image computing and computer-assisted intervention*, Springer. pp. 234–241.
- [71] Sarker, M.M.K., Rashwan, H.A., Akram, F., Banu, S.F., Saleh, A., Singh, V.K., Chowdhury, F.U., Abdulwahab, S., Romani, S., Radeva, P., et al., 2018. Slsdeep: Skin lesion segmentation based on dilated residual and pyramid pooling networks, in: *International Conference on Medical Image Computing and Computer-Assisted Intervention*, Springer. pp. 21–29.
- [72] Savelli, B., Bria, A., Molinara, M., Marrocco, C., Tortorella, F., 2020. A multi-context cnn ensemble for small lesion detection. *Artificial Intelligence in Medicine* 103, 101749.
- [73] Scheffe, H., 1999. *The analysis of variance*. volume 72. John Wiley & Sons.
- [74] Serte, S., Demirel, H., 2019. Gabor wavelet-based deep learning for skin lesion classification. *Computers in biology and medicine* 113, 103423.
- [75] Shahin, A.H., Kamal, A., Elattar, M.A., 2018. Deep ensemble learning for skin lesion classification from dermoscopic images, in: *2018 9th Cairo International Biomedical Engineering Conference (CIBEC)*, IEEE. pp. 150–153.
- [76] Siegel, R.L., Miller, K.D., Jemal, A., 2020. Cancer statistics, 2020. *CA: A Cancer Journal for Clinicians* 70, 7–30.
- [77] Song, L., Lin, J.P., Wang, Z.J., Wang, H., 2020. An end-to-end multi-task deep learning framework for skin lesion analysis. *IEEE Journal of Biomedical and Health Informatics* .
- [78] Srivastava, N., Hinton, G., Krizhevsky, A., Sutskever, I., Salakhutdinov, R., 2014. Dropout: a simple way to prevent neural networks from overfitting. *The journal of machine learning research* 15, 1929–1958.
- [79] Szegedy, C., Vanhoucke, V., Ioffe, S., Shlens, J., Wojna, Z., 2016. Rethinking the inception architecture for computer vision, in: *Proceedings of the IEEE conference on computer vision and pattern recognition*, pp. 2818–2826.
- [80] Tan, M., Le, Q.V., 2019. Efficientnet: Rethinking model scaling for convolutional neural networks. *arXiv preprint arXiv:1905.11946* .
- [81] Tang, Y., Yang, F., Yuan, S., et al., 2019. A multi-stage framework with context information fusion structure for skin lesion segmentation, in: *2019 IEEE 16th International Symposium on Biomedical*

- Imaging (ISBI 2019), IEEE. pp. 1407–1410.
- [82] Torrey, L., Shavlik, J., 2010. Transfer learning, in: Handbook of research on machine learning applications and trends: algorithms, methods, and techniques. IGI Global, pp. 242–264.
- [83] Valle, E., Fornaciali, M., Menegola, A., Tavares, J., Bittencourt, F.V., Li, L.T., Avila, S., 2020. Data, depth, and design: Learning reliable models for skin lesion analysis. *Neurocomputing* 383, 303–313.
- [84] Venugopal, A., Stoffel, E.M., 2019. Colorectal cancer in young adults. *Current treatment options in gastroenterology* 17, 89–98.
- [85] Xie, F., Yang, J., Liu, J., Jiang, Z., Zheng, Y., Wang, Y., 2020a. Skin lesion segmentation using high-resolution convolutional neural network. *Computer Methods and Programs in Biomedicine* 186, 105241.
- [86] Xie, Y., Zhang, J., Xia, Y., Shen, C., 2020b. A mutual bootstrapping model for automated skin lesion segmentation and classification. *IEEE Transactions on Medical Imaging* .
- [87] Yadav, S.S., Jadhav, S.M., 2019. Deep convolutional neural network based medical image classification for disease diagnosis. *Journal of Big Data* 6, 113.
- [88] Yilmaz, E., Trocan, M., 2020. Benign and malignant skin lesion classification comparison for three deep-learning architectures, in: *Asian Conference on Intelligent Information and Database Systems*, Springer. pp. 514–524.
- [89] Yu, Z., Jiang, F., Zhou, F., He, X., Ni, D., Chen, S., Wang, T., Lei, B., 2020. Convolutional descriptors aggregation via cross-net for skin lesion recognition. *Applied Soft Computing* , 106281.
- [90] Yuan, Y., 2017. Automatic skin lesion segmentation with fully convolutional-deconvolutional networks. *arXiv preprint arXiv:1703.05165* .
- [91] Zhang, J., Xie, Y., Xia, Y., Shen, C., 2019. Attention residual learning for skin lesion classification. *IEEE transactions on medical imaging* 38, 2092–2103.
- [92] Zhang, N., Cai, Y.X., Wang, Y.Y., Tian, Y.T., Wang, X.L., Badami, B., 2020. Skin cancer diagnosis based on optimized convolutional neural network. *Artificial Intelligence in Medicine* 102, 101756.